筑　波　大　学

博 士 （ 医 学 ） 学 位 論 文

Gold nano-particles as radiosensitizers for glioma radiotherapy

グリオーマの放射線治療に向けての

放射線感受性金ナノ粒子の開発

2013

筑波大学大学院博士課程人間総合科学研究科

Zaboronok Alexander

ACKNOWLEDGEMENTS

In this work I would like to thank my academic advisor Professor Akira Matsumura for his support during my research at the Department of Neurosurgery, University of Tsukuba, and my advisor in the gold nanoparticles project, Associate Professor Hideo Tsurushima, for his ideas, supervision and help with the publication preparation. I would also like to thank all the staff of the Department of Neurosurgery, especially Makiko Miyakawa, Yoshiko Tsukada and Fumiyo Yoshida for their technical assistance. I would also like to thank the following people: Takeji Sakae, Tomonori Isobe and Kenta Takada (Proton Medical Research Center, University of Tsukuba) for their assistance in X-ray radiation source calibration; Professor Jong-Ki Kim (Catholic University of Daegu, South Korea), Sergey Uspenskiy (International Research center "Martinex", Moscow, Russian Federation), Andrey Mishchenko (RIKEN, Tokyo, Japan), Alexander Aryshev (KEK, High Energy Accelerator Research Organization, Tsukuba, Japan) and Ivan Turkevych (NIMS, National Institute for Materials Science, Tsukuba, Japan) for their help in understanding physical and chemical aspects related to gold nanoparticles; Flaminia Miyamasu and Brian K. Purdue (MECC, University of Tsukuba) for their native English language assistance. I would like to thank my wife, Nadzeya Kavaliova, who left her job in Belarus to share with me life in Japan, for her understanding and help with our small children, Alisa and Andrey, while I devoted most of my time to the research and work.

This work was partly supported by Grants-in-Aid for Scientific Research (B), No. 22360040, and (C), No. 23592085, from the Ministry of Education, Culture, Sports, Science, and Technology-Japan (MEXT).

List of abbreviations

ANOVA: analysis of variance

ATCC: American Type Culture Collection

AUC: area under curve

CT: computer tomography

D: (irradiation) dose

D_{10}: dose needed to achieve 10% of the cell survival

DDS: drug delivery system

DEF: dose enhancement factor

DNA: deoxyribonucleic acid

EPR: enhanced permeability and retention (effect)

FBS: fetal bovine serum

GBM: multiform glioblastoma

GNPs: gold nanoparticles

Gy: gray

HAMG-GNPs: hyaluronic acid-melanin-based gold nanoparticles

ICP-MS: inductively coupled plasma mass-spectrometry

LN: natural logarithm

LQ: linear–quadratic (model)

MEM: minimum essential medium

MTS: 3-(4,5-dimethylthiazol-2-yl)-5-(3-carboxymethoxyphenyl)-2-(4-sulfo-phenyl)-2H-tetrazolium

p53: tumor suppressor protein

PBS: phosphate buffer saline

PCT: photon capture therapy

PE: plating efficiency

PMS: phenazine methosulfate

SD: standard deviation

SF: cell survival fraction

SF_2: surviving fraction at 2Gy

TEM: transmission electron microscopy

U251MG: U251 malignant glioma

UV: ultraviolet

W: (statistical) weight

CONTENTS

Part I: U251MG cell radiosensitization with 8 and 50 nm gold nanoparticles

Part II: Hyaluronic acid-melanin-based GNPs

PART I: U251MG CELL RADIOSENSITIZATION WITH 8 AND 50 NM GOLD NANOPARTICLES

1. INTRODUCTION

Modern techniques and knowledge in chemistry and biochemistry allow working with matter at a nanoscale level. Regarding medical sciences, such an approach is especially beneficial for oncology, where exclusive influence on tumor cells spread in normal tissues can provide necessary conditions for cancer treatment (Cuenca et al 2006, Rao 2008, Cai et al 2008). When the size of cells is scaled in μm, we need even smaller agents working at the level of organelles or even the molecular level for selective cancer cell therapy; and such intervention has to be more intelligent than just physical or chemical influence. Thus, without interfering at the nanoscale level, modern oncology with its latest surgical techniques, newly developed advanced chemotherapy agents and various radiation sources, fails to cure patients with certain types of malignant tumors.

In neuro-oncology, such nanoscale influence is vital for the treatment of gliomas, and especially GBM (grade IV glioma, according to World Health Organization classification), the most malignant glioma, characterized by fast and invasive growth (Guillamo et al 2001, Lefranc et al 2005, Furnari et al 2007). It is among those incurable cancers with poor quality of life and poor prognosis, and most GBM patients die of their disease with a median survival of one year, despite using all modern treatment modalities (Lefranc et al 2005, Hoelzinger et al 2007, Matsuda et al 2011). As radiotherapy remains one of the most commonly used adjuvant modalities in glioma treatment, the realization of a nanoscale influence might be connected with the use of nanoparticles not only as carriers of medical drugs or antibodies, but also as radiosensitizers - enhancers of the ionizing radiation effect within tumor cells (Carter et al 2007, Cai et al 2008, Rahman et al 2010, Jelveh and Chithrani 2011).

Radiosensitization was established long before the development of nanotechnology. Thus, the difference in the absorbed dose in biological tissues after X-ray irradiation was observed at the interface of materials with different atomic numbers (Z) (Spiers 1949). An additional effect of radiation was also found in tissues with X-ray contrast agents (Adams et al 1977, Callisen et al 1979, Santos Melloet al 1983), and it was suggested that certain compounds could be used to locally enhance the radiation dose. Different non-metallic chemical substances were tested for radiation enhancement (Biaglow et al 1983, Nath et al 1990, Murayama et al 1993, Nishioka et al 1999, Shibamoto et al 2001), as well as X-ray contrast agents, mainly based on iodine (Matsudaira et al 1980, Fairchild et al 1983, Rose et al 1999, Karnas et al 1999, Robar et al 2002, Corde et al 2004, Boudou et al 2005, Esteve et al 2006, Adam et al 2006). Recent studies on dose perturbations at interfaces with high-Z materials in kilovoltage and megavoltage photon beams (Das and Kahn 1989, Das and Chopra 1995) and more relevant secondary radiation from metallic gold surfaces at the interface with biological structures (Regulla et al 1998 and 2002) showed higher potential of high-Z metals, and especially gold, in comparison with non-metallic compounds. In this regard, golden microspheres were introduced as biologically effective radiosensitizers (Herold et al 2000), and with the development of nanotechnology, nanoparticles made of materials with different atomic numbers (25 to 90) were tested for radiosensitization (Roeske et al 2007).

Gold has certain advantages in comparison with other radiosensitizers, such as iodine or gadolinium (Cho 2005), which have already been approved and used in clinical practice as contrast agents. Gold nanoparticles can provide a higher degree of radiation enhancement with relative chemical inactivity in living organisms, which predetermines higher doses of gold used within the safety level (Cai et al 2008, Jelveh

and Chithrani 2011). Radiation enhancement using GNPs is mainly determined by Auger electrons and secondary (fluorescent) photons emitted from the irradiated particles. For such interactions tumor cells containing GNPs should be irradiated with X-ray photons with energies over those of the inner K (68.0–80.7 keV), L (L1 14.4 keV; L2 13.7 keV; L3 11.9 keV) and M (2.2–3.4 keV) gold atomic shells, which are sufficient to eject electrons from the mentioned orbits (Figure 1) (Leung et al 2011). As such reactions are related to photon capture by gold atoms, therapy using this method can be defined as a photon capture therapy (PCT). The influence of X-rays on GNP-containing tumor cells can be described in several parallel and consecutive processes (Figure 2), which include electron and photon emission from irradiated GNPs (direct influence) and the production of free radicals from GNPs-emitted photons and electrons (indirect influence) (Han et al 2010, Jelveh and Chithrani 2011).

The plasticity of gold as a main component of nanoparticles enables the production of nano-sized structures of different forms, including gold nano-rods, nano-cages, and nano-shells (Wei and Zamborini 2004, Rodriguez-Fernandez et al 2005, Cai et al 2008, Jelveh and Chithrani 2011). In comparison with such structures, round-shaped GNPs are most commonly used in oncological research mainly because of their relatively easy production, lower toxicity and greater capacity for functionalization (Cai et al 2008, Chithrani et al 2006, 2010 and 2011, Pan et al 2007, Rahman et al 2009, Butterworth et al 2010)

Therefore, in our study we tested the radiosensitization efficacy of round-shaped GNPs on human U251MG cells. We used 8 nm GNPs, as <10 nm particles were theoretically described as capable of tumor cell nuclei penetration (Chithrani et al 2010), and 50 nm GNPs, as particles of such size were reported to be best accumulated by

tumor cells (Chithrani e al 2006 and 2010). Parameters such as light absorption, cytotoxicity and uptake by tumor cells, were also evaluated.

2. STUDY OBJECTIVES

1. Evaluate optical properties of 8 and 50 nm GNPs in PBS solution based on light absorption characteristics.
2. Determine intracellular localization, cytotoxicity and cellular uptake of 8 and 50 nm GNPs in human U251MG cells.
3. Evaluate radiotherapy the enhancement effect of GNPs in different concentrations in human U251MG cells.

3. MATERIALS AND METHODS

3.1 Gold nanoparticles

Colloidal solutions of oligoglycine-stabilized 8 and 50 nm GNPs containing 750 and 500 ppm of gold, respectively, were purchased from Winered Chemical, Inc., Tokyo, Japan (http://www.winered.jp). The particles were produced by the method described elsewhere (Watabe 2005). The size of GNPs was declared by the manufacturer. The light absorption was estimated on a UV-2501 PC® optical analyzer (Shimadzu Co. Ltd., Kyoto, Japan). The amount of gold in the particle colloidal solution was reassessed by the inductively coupled plasma mass-spectrometry (ICP-MS). GNPs were maintained in sterile tubes at 4°C.

3.2 U251MG cell line

Human U87MG cells were obtained from ATCC and cultured at 37°C in a humidified atmosphere of 5% CO2 in MEM (M4655, Sigma-Aldrich, MO, USA) supplemented with 10% fetal bovine serum (FBS; JRH Nichirei Biosciences, Tokyo, Japan) and 1% penicillin-streptomycin (100 U/ml penicillin, 0.1 mg/ml streptomycin, Sigma-Aldrich, MO, USA).

3.3 X-ray source

The Hitachi MBR-1520R biological X-ray irradiator, operated at 150kVp and 20mA, was calibrated using an AE1341-D ionizing chamber (Applied Engineering, Inc., Tokyo, Japan) and GD-352M glass dosimeters (AGC Techno Glass Co., Ltd., Chiba, Japan), analyzed by a KXO-50XM X-ray diagnostic system (Toshiba Medical Systems, Co.). Glass dosimeters were placed in the center and 40 mm from the center of

the rotating table, at a distance of 350 mm from the X-ray tube; dosimetry results were further used for dose adjustment. The spectrum of the irradiator was simulated by SpekCalc® software using Poludniowsky algorithm (Poludniowsky et al 2007, 2009) (Figure 3).

3.4 Transmission electron microscopy

The size and localization of GNPs in U251MG cells were studied using a JEM-1400 transmission electron microscope (JEOL Ltd., Tokyo, Japan) operated at an accelerating voltage of 120 kV. U251MG cells were incubated with 8 and 50 nm GNPs at a gold concentration of 15 μg/ml during 24 h. After incubation, cells containing nanoparticles were washed twice with PBS, centrifuged, fixed and submitted for further processing. The samples were mounted on copper grids, placed into the TEM. The images were analyzed to determine the particle size and intracellular localization.

3.5 Cytotoxicity assay

The cytotoxicity evaluation was performed to show the decrease in cell proliferation after incubation with GNPs in order to determine the maximum gold concentration in the medium applicable for further experiments. In short, 100 μl of MEM with 8000 of U251MG cells was placed in each well of 96-well plates and incubated for 24 h. The medium was replaced by MEM with GNPs (15 - 150 μg gold/ml) and further incubated for 24 h. Then, the medium containing GNPs was removed, and the cells were washed twice with PBS. 2 ml of a 3-(4,5-dimethylthiazol-2-yl)-5-(3-carboxymethoxyphenyl)-2-(4-sulfophenyl)-2H-tetrazolium (MTS) solution with PMS (Cell Titer 96® AQueous One Solution, Promega, WI, USA) were mixed with 10 ml of MEM, and added in the amount of 100 μl to each well. The cells without GNPs were used as controls. The plates were incubated and the absorption at 490 nm

was assessed using a Mithras LB 940 Multimode reader (Berthold Technologies, Germany) after 2 h. As GNPs are visually non-transparent and may disturb light absorption, the wells containing cells with GNPs without MTS solution were used as additional controls.

3.6 Gold accumulation by U251MG cells

The accumulation of gold in GNPs by the tumor cells was assessed with the ICP-MS (ICP-8100MS, Shimadzu, Kyoto, Japan) according to the protocol, modified from the methods described elsewhere (Martin de Llano et al 1996, Scheffer et al 2008, Allabashi et al 2009, Furuyama et al 2009 and Judy et al 2011). In short, after the incubation in 4 ml of MEM with GNPs at different concentrations (15 - 45 μg gold/ml) the cells were washed twice with PBS, detached from the flasks with 0.05% trypsin-EDTA (Nacalai Tesque, Inc., Japan), counted, and heated at 120°C in the concentrated nitric acid for 2 h. The necessary amount of the hydrochloric acid was added to obtain Aqua Regia to dissolve gold. The solution was diluted with distilled water, filtrated with 50 μm filters and submitted for the ICP-MS. The amount of gold was recalculated for 10^6 cells.

3.7 Radiation treatment & Colony forming assay

U251MG cell survival after X-ray irradiation was assessed by colony forming assay. Initially, U251MG cells were seeded at a concentration of 10^6 cells per flask and incubated for 24 hours. 8 or 50 nm GNPs were diluted in MEM to the gold concentrations of 15 μg/ml, 30 μg/ml and 45 μg/ml, the medium in the flasks was replaced with a new medium containing GNPs, and the cells were further incubated during 24 h. After incubation, the cells were washed twice with PBS, separated into different plastic tubes according to the gold concentration and irradiation dose, and

irradiated with 2, 4 and 8 Gy. Treated-with-GNPs unirradiated cells, untreated irradiated and untreated unirradiated cells were used as controls. After irradiation, U251MG cells were diluted and placed into round plates according to the irradiation dose and the concentration of GNPs, and incubated for 14 days. After incubation, cells were fixed and stained with 0.2% crystal violet. The plates were scanned and the colonies of over 50 cells were counted using Biozero® software (Keyence, IL, USA).

3.8 Evaluation of radiobiological parameters

All the experiments were repeated at least 3 times each; colony forming assay results were summarized from at least four independent experiments. The cytotoxicity, gold accumulation and cell survival data represent means ± SDs, p-values were calculated by one-way ANOVA. In the colony forming assay, the cell survival fraction (SF) was calculated as follows:

$$SF = \frac{no.colonies\ after\ irradiation\ with/without\ GNPs}{no.of\ seeded\ cells \times PE},$$

where the plating efficiency (PE) was obtained from the equation:

$$PE = \frac{no.of\ colonies\ without\ treatment}{no.of\ seeded\ cells}.$$

To determine the linear parameter α and the quadratic parameter β, the cell survival curves were fitted by a weighted, stratified, linear regression function in SPSS 18.0 (PASW Statistics 18, IBM, NY, USA) according to the linear–quadratic formula: $SF = e^{-(\alpha D + \beta D^2)}$, where D is the irradiation dose, using the protocol, adapted from elsewhere (Franken et al 2006). In the regression, SF was assigned as a dependent variable, D and D^2 as independent variables, and the statistical weight was estimated as follows:

$$W = \frac{no.of\ the\ colonies \times no.of\ seeded\ cells}{no.of\ seeded\ cells - no.\ of\ colonies}.$$

Statistical errors of α and β were calculated with 95% confidence intervals. Using α and β values such parameters as SF_2 dose and D_{10} were calculated for each gold concentration and irradiation dose by solving the quadratic equation:

$$ax + bx^2 + ln(SF) = 0,$$

where *a*=α, *b*=β, *c*=ln(SF), and *x* represented the dose and equaled:

$$x = \frac{-a \pm \sqrt{a^2 - 4bc}}{2b};$$

positive values of x were used. SF_2 dose represented the irradiation dose delivered to the cells with GNPs needed to obtain the same surviving fraction as 2 Gy irradiation given to the cells without GNPs, and D_{10} was the dose needed to achieve 10% of the cell survival. Dose enhancement factors were calculated as ratios of the control parameters to the treatment parameters. Thus, DEF (SF_2) was the ratio of the control 2 Gy to the SF_2 dose, and DEF (D_{10}) was the D_{10} ratio between the controls and cells with GNPs. P-values (SF_2 fit.) were calculated from the fitted values of SF_2. AUC was the area under each fitted LQ model curve, and was calculated to determine the statistical significance between the control and treatment curves as a definite integral of the linear quadratic function:

$$AUC = \int_0^8 \exp(-\alpha x - \beta x^2)\, dx\,;$$

DEF (AUC) was the AUC ratio between the control and treatment curves, *x* was the dose.

4. RESULTS

4.1 Light absorption by GNPs

Normalized light absorption spectra of 8 and 50 nm GNPs colloidal solutions are presented in Figure 4. There are single peaks for each type of particles with the maximum light absorption at 522 nm for 8 nm GNPs and 530 nm for 50 nm GNPs, and the narrower peak of 50 nm GNPs.

4.2 Transmission electron microscopy

On TEM images, 8 nm and 50 nm GNPs were clearly seen in the cytoplasm of glioma cells (Figure 5A,B). The 8 nm particles looked more uniform in their size and more intense accumulation in tumor cells was observed; it was clearly seen that the cells captured 8 nm particles into vesicles. The diameter of larger GNPs varied; both types of particles were seen only in the cytoplasm of the examined cells, without obvious nuclei penetration.

4.3 Cytotoxicity of gold nanoparticles

The decrease in proliferation of U251MG cells was related to the concentration of GNPs in the medium (Figure 6). The concentration of 15, 30 and 45 μg gold/ml of both types of GNPs did not significantly reduce cell proliferation compared to the control. The presence of 8 nm GNPs in concentrations over 45 μg gold/ml significantly decreased cell proliferation; the proliferation of cells containing 50 nm GNPs did not significantly differ from the control within the studied gold concentration range (15-150 μg gold/ml). For 8 nm GNPs, cell proliferation decreased from 68±11% at 60 μg

gold/ml to 30±18% at 150 μg gold/ml. The concentration of 15, 30 and 45 μg gold/ml of both GNPs was used in further experiments.

4.4 Accumulation of gold by the tumor cells

The amount of gold accumulated in 10^6 of U251MG cells evaluated by the ICP-MS is presented in Figure 7. Gold accumulation varied depending on the initial GNPs concentration in the medium. Thus, at 15 μg gold/ml in MEM larger 50 nm GNPs showed 1.27 times higher gold accumulation than 8 nm GNPs (17.11±1.26 versus 13.50±0.49, p=0.01). At higher concentrations, cells with 8 nm GNPs showed higher gold accumulation. Thus, at 30 μg gold/ml 8 nm GNPs showed 1.31 times higher gold accumulation than 50 nm GNPs (37.66±1.61 versus 28.72±0.41, p=0.001) and at 45 μg gold/ml 1.30 times higher gold accumulation (53.74±2.79 versus 41.43±0.88, p=0.001).

4.5 Glioma cell survival and dose enhancement

Colony forming abilities of U251MG cells were assessed in 10 consecutive X-ray irradiation experiments, and the normal survival data (without GNPs) were fitted to the LQ model using the regression function, as described in Materials and Methods, and presented in Figure 8. The parameters α and β were determined from the curve fit as 0.196±0.002 and 0.027±0.0004, respectively. Using these parameters the dose needed for 10% cell survival (D_{10}) was calculated and equaled 6.132±0.694 Gy. The area under curve (AUC) was evaluated to compare the difference between the treatment and control curves (Figure 9) and equaled 2.897±0.431 (the relative area). The survival curves of glioma cells with GNPs were estimated using the data of at least 4 experiments, fitted similarly to the control and presented in Figures 10 A, B. The parameters α and β, SF_2 doses, D_{10}, AUCs, DEFs and the p-values of the control and treatment groups of cells are arranged in Table 1.

5. DISCUSSION

5.1 Optical properties of GNPs

Optical properties of GNPs in colloidal solutions obtained from Winered Chemical laboratory were studied to verify the presence of nano-sized particles and their stability in the solution before using them in experiments on cells. The presence of nano-sized particles in the solution was confirmed by the spectrum of light absorption with an obvious peak at a certain wavelength for each particle type (522 nm for 8 nm GNPs and 530 nm for 50 nm GNPs, Figure 4). The formation of the absorption peak is determined by a well-known phenomenon called plasmon resonance, which is related to the presence of surface electromagnetic waves at the interface of a metal and dielectric material (Bohren and Huffman 1983, Kreibig and Vollmer 1995). The essence of this phenomenon is the resonance of the internal collective oscillations of electrons in metal with the oscillations generated by the electromagnetic wave spreading in the medium (water solution, or PBS in our case). The plasmon absorption band emerges when the size of particles becomes smaller than the length of the free pass of free electrons in the metallic mass (several nanometers to several tens of nanometers). The scattering of free electrons takes place mainly at the surface of particles, therefore the plasma frequency of free oscillations of electrons shifts from the UV range to the visible light spectrum, and we can see the peak of absorption if there are nanoparticles in the solution. Thus, with the presence of single peaks for each type of GNPs at the different wavelengths, we confirmed that we had stable colloidal solutions of nanoparticles with different sizes, suitable for further cell experiments, and the narrower peak of 50 nm GNPs represented more uniform particle size distribution.

5.2 Size and localization of GNPs in tumor cells

Visualization with TEM confirmed the ability of the tumor cells to capture GNPs by the elongations, and both 8 and 50 nm GNPs were clearly seen in the cytoplasm of U251MG cells (Figure 5 A, B). It is considered that smaller < 10 nm GNPs have a potential to penetrate the nuclei of cells, providing better opportunities for radiation therapy when located close to the DNA (Chithrani et al 2010). Nevertheless, both types of GNPs were well observed in the vesicles within the cell cytoplasm, without obvious nuclei penetration, as it was not clearly seen if single particles were separated from the clusters and located in other cell organelles or penetrated the nuclei. The use of GNPs < 8 nm could theoretically increase the probability of nuclei penetration, though even smaller sizes of particles may lead to a significant decrease in the cell uptake, determining the necessity of using particle carriers, such as liposomes, to achieve essential accumulation in cells (Chithrani et al 2010). The size of particles was also evaluated using TEM, though the most contrasting part of a particle was the central cluster of gold atoms, and the outer layer of the stabilizing compound might not be clearly visible.

5.3 Composition and cytotoxicity of GNPs

To be used in living organisms for radiation enhancement, nanoparticles need to combine high radiosensitization properties with biocompatibility. Among different forms, spherical nanoparticles were most commonly used by researchers in the field of medical physics and oncology, because of stability and relative biological inertness of such nanostructures (Chang et al 2008, Kim et al 2010, Chithrani et al 2010, Jain et al 2011). There are several reasons for using spherical GNPs, and the first one is the easiest way of particle production, where in many cases gold is stabilized by the salts of

citric acid, or citrates (Cai et al 2008, Hainfeld et al 2004, 2006, 2008 and 2010, Chithrani et al 2006 and 2010, Butterworth et al 2010, Chithrani 2011), and the size of particles depends on the amount of ionized gold included in the chemical reaction. Another reason to use a spherical shape may be connected with the intention to reduce the toxicity of GNPs. In contrast to previous suggestions about the absolute inertness of gold in biological systems, recent studies have shown structure- and size-dependent toxicity of GNPs (Pan et al 2007, Butterworth et al 2010, Jain et al 2011, Trono et al 2011). Finally, the spherical shape provides the possibility to uniformly cover the round particle surface with active compounds, such as polysaccharide molecules, medical drugs, antibodies or fluorescent components, for specific targeting of cells or tissues (Chen and Zhang 2006, Kong et al 2008).

In our study, we used oligoglycine-stabilized spherical GNPs, which showed size-dependent cytotoxicity (Figure 6). According to the literature data, the cytotoxicity of gold nanoparticles depends on their size and their concentration in the medium (Pan et al 2007, Butterworth et al 2010). Nevertheless, 50 nm GNPs were not toxic for U251MG cells within the studied concentration range, whereas 8nm GNPs decreased cell proliferation significantly at concentrations over 45 μg/ml. Thus, only 8 nm particles corresponded to the concentration-dependent cytotoxicity model.

We assumed that, in the case of spherical GNPs, the toxicity might be related to the potential presence of a layer of ionized gold, located between the inert metallic golden core with 0-valency and the layer of the stabilizing component (e.g., citrate or amino-acid layer). Thus, the toxicity may depend on the surface reactivity, related to the ability of the non-reactive surface layer to hide the reactive ionized gold. Therefore, in our experiments larger 50 nm GNPs could be less toxic due to the thicker layer of glycine oligopeptide on their surface hiding the reactive ionized gold.

It could also be possible to use the additional toxic effect of 8 nm GNPs in cancer therapy, though specific protection of normal cells would be needed, such as encapsulation of such particles into liposomes or other carriers, and even in that case it would be risky for normal tissues. So such an approach requires further investigation.

The non-toxic gold concentration range was assigned as 15 to 45 μg/ml, and all further experiments were performed using these concentrations. In regard to the atypical cytotoxicity results, we can suggest, that not only size, but the composition of GNPs may play a role, as well as other factors yet to be studied.

5.4 Accumulation of GNPs by U251MG cells

According to the literature data, 50 nm GNPs show the highest cell accumulation (Chithrani et al 2006). Nevertheless, in our study the accumulation of GNPs varied depending on the initial concentration in MEM (Figure 7). Thus, 50 nm GNPs showed better cell uptake at 15 μg/ml, and 8 nm GNPs showed better cell uptake at 30 and 45 μg/ml. There could be some relationship between higher accumulation of 8 nm gold nanoparticles in cells (at 30 and 45 μg/ml) and their higher cytotoxicity level. Thus, more detailed studies are required to determine such a relationship.

We suggest that not only size, but the combination of factors, including form, size and composition of GNPs, might be responsible for particle accumulation in vitro. Moreover, in vitro experiments can only partially correspond to animal tumor models, and in some cases do not represent the real state of events. The enhanced permeability and retention (EPR) effect contributes to the delivery of GNPs to the tumor tissue through leaky tumor vessels (Dvorak et al 1988, Maeda et al 2000, Furuyama et al 2009). We suggest that the presence of GNPs around the tumor cells in the animal

model or in real clinical conditions can be provided mostly by particle functionalization, leading to targeted delivery.

5.5 X-ray irradiation source and photon capture by GNPs

Energies necessary to induce the GNPs-related radiotherapy enhancement were described according to theoretical calculations and computer software simulations (Leung et al 2011, Brun et al 2009, Montenegro et al 2009, Pradhan et al 2009). In most cases, the photon capture and electrons/photons emission takes place when the initial X-ray influence is provided within the kilo electron volt (keV) energy range. The influence of higher photon energies, e.g. within the mega electron volt (MeV) range, initiates different processes, mainly connected with photon scattering, and the radiation enhancement effect is lower than that at the keV-irradiation (Jain et al 2011, Leung et al 2011). And within the keV range the influence on Kα-edge with the energy of 68 keV or slightly higher was suggested to be more efficient for GNPs-related radiosensitization (Montenegro et al 2009, Pradhan et al 2009).

The irradiation source we used could provide only a limited amount of photons in the effective energy range, as the conventional X-ray tube contained a wide spectrum of photon energies (Figure 3). Nevertheless, it is possible to determine the most advantageous irradiation energies according to the X-ray mass attenuation coefficients of gold and other materials presented by the US National Institute of Standards and Technology (http://www.nist.gov/pml/data/xraycoef/index.cfm). We studied the compliance of the spectrum of Hitachi MBR-1520R biological X-ray irradiator, designed by SpekCalc® software using Poludniowsky algorithm (Poludniowski et al 2007, 2009), with the energies needed to eject electrons from gold atom inner shells. Thus, in our case the effective parts of the spectrum with the excess of energies of the

initial photons over that of K-, L, and M-shells represent the potential energy of secondary photons, emitted by gold atoms, as well as the pathway length of ejected Auger electrons.

GNPs absorb a portion of the initial X-rays and emit low energy electrons and secondary (fluorescent) photons, which were previously found to damage DNA and the cell microenvironment (Boudaiffa et al 2000, Sanche 2002, Brun et al 2009). Indirect damage to DNA and the cell organelles by free radicals (mainly OH*), produced from GNPs-emitted low energy electrons and photons interacting with water molecules may also take place, as such interactions were discovered long before the invention of GNPs (Chatterjee and Magee 1985) and further investigated in recent years (Sanche 2009, Wang et al 2009). When local interactions take place within micrometers, secondary photons and electrons have the potential to damage cell DNA or other cell components, such as cell membranes (e.g., through lipids peroxidation). Nevertheless, if the initial X-ray energy is low, the secondary processes may take place within nanometers, and to damage DNA GNPs need to be located in close proximity to chromosomes, very close or within the cell nucleus, which can theoretically be achieved only by using very small < 10 nm particles. However, very small (several nm) size of GNPs may lead to decrease in particle uptake and higher toxicity; so particle incorporation in larger carriers, such as liposomes, would be required (Chithrani et al 2010).

5.6 Glioma cell radiosensitization and dose enhancement factors

Survival data of irradiated U251MG cells showed the typical influence of ionizing radiation on the colony forming abilities of tumor cells with the compliance of fitted curves to the LQ model (Figure 8). The linear-quadratic model was first proposed by Douglas and Fowler (1976) and now is the most commonly used model to describe

the effect of ionizing radiation on cells. In such a representation, the single destructive event or influence of radiation is described by the alpha-parameter, which is linearly related to dose, and the two-stage mechanism of DNA destruction is related to the square of the dose (beta-parameter). Therefore, the linear quadratic model corresponds to double strand DNA breaks, which are responsible for cell destruction by ionizing radiation. The use of the linear-quadratic model is described in the classical protocol of colony forming assay, which was used in our study (Franken at al., 2006). The curve fit allowed determination of the linear parameter α and the quadratic parameter β, which characterized the exponential decrease in cell survival after irradiation in small doses, and to evaluate the significance of differences between the treatment and control curves finding AUC - the area under the LQ fitted curves (Figure 9). We observed that X-ray irradiation with 8 Gy within the spectrum of MBR-1520R biological irradiator in combination with 8 nm GNPs in the concentration of 45 μg/ml and 50 nm GNPs in concentrations of 30 and 45 μg/ml could provide effective tumor cell growth control (Figure 10 A, B). To analyze the additional effect of secondary radiation from GNPs and calculate dose enhancement factors (DEFs), such parameters as the dose needed for 10% cell survival and the SF_2 dose were calculated using α and β values (Table 1), as described in the literature (Butterworth et al 2010, Jain et al 2011). In our study we used radioresistant p53-mutant human U251 malignant glioma cells, which are characterized by p53-independent apoptosis (Afshar et al 2006) and cell cycle arrest was observed after irradiation. As p53-independent apoptosis is more prominent after irradiation with higher doses (Merritt et all 1997), we observed insignificant differences between 2 Gy irradiation values of the control and treatment groups using both types of GNPs (Figure 10 A, B). Similarly, SF_2 dose values and the corresponding dose enhancement factors DEF (SF_2) were found not significant, whereas D_{10}, AUC and the

corresponding DEF (D_{10}) and DEF (AUC) values were found to be statistically reliable factors to assess radiation enhancement (Table 1). AUC and the corresponding DEF (AUC) values represented the general behavior of the cell survival curves within the irradiation range (0 - 8 Gy). D_{10} and DEF (D_{10}) were found statistically more significant than other parameters, as p-values were lower than those for other radiobiological parameters (Table 1). From the experimental data, effective radiosensitization of glioma cells was achieved at 8 Gy of keV-X-ray irradiation of the cells with 8 nm GNPs using 45 μg gold/ml in the medium (p=0.024); 50 nm particles showed more significant radiosensitization at 8 Gy with 30 μg gold/ml (p=0.006) and 45 μg gold/ml (p=0.006) (Figure 10 A, B).

Based on gold accumulation and cell survival data we can summarize that at least 8 Gy X-ray irradiation of glioma cells containing at least 53.7 μg of gold per 10^6 cells in the form of 8nm GNPs and 28.7-41.4 μg of gold per 10^6 cells in the form of 50nm GNPs can provide tumor growth control. Due to the toxicity of 8 nm GNPs, 50 nm GNPs are more suitable for radiosensitization and eligible for further studies.

Our work clarified certain processes that happen when gold nanoparticles are accumulated by tumor cells and irradiated with X-rays. We believe that the results of our study will be useful for other researchers in the same field and may help further development of cancer radiotherapy.

6. CONCLUSION

1. 8 nm and 50 nm GNPs were present in stable colloidal solutions and showed optical properties typical for nano-sized spherical particles.
2. Both types of GNPs were captured by U251MG cells by the invaginations of the cell membrane, and clustered into vacuoles in the cytoplasm of glioma cells, without obvious nuclei penetration.
3. Both types of GNPs were well accumulated in U251MG cells: smaller 8 nm particles showed higher cytotoxicity, whereas 50 nm GNPs were non-toxic within the studied concentration range (15 - 150 μg/ml).
4. Both types of GNPs provided radiotherapy enhancement for human U251 malignant glioma cells at certain concentrations (at 45 μg/ml of 8 nm particles and 30 - 45 μg/ml of 50 nm particles) irradiated with 8 Gy of 150 kVp X-rays; for p53-mutant U251MG cells, D_{10} and AUC were found to be statistically reliable parameters to evaluate dose enhancement.
5. 50 nm GNPs might have a higher potential in glioma radiotherapy enhancement, and further studies in this area, including active tumor targeting with GNPs, are required to evaluate the efficacy of this method.

PART II: HYALURONIC ACID-MELANIN-BASED GNPS

7. INTRODUCTION

Cancer diagnosis and therapy can be better provided using functionalized agents, aimed to target specific cells, tissues or organs. Such an approach is suggested to be more beneficial than the enhanced permeability and retention (EPR) effect, which contributes to non-specific accumulation of nanoparticles in tumor cells through fenestrated tumor vessels (Dvorak et al 1988, Maeda et al 2000, Furuyama et al 2009). Additionally, fixation of nanoparticles in the tumor tissue after targeted delivery might prolong the effect of therapy and contribute to better prognosis.

In this regard, we proposed the use of melanin and hyaluronic acid, included into the particle composition, to improve the functional potential of GNPs (Figure 11). Melanin molecules can bind to and imbed a large number of gold atoms, providing high gold concentration relative to other compounds, and hyaluronic acid (HA) is designed to provide fixation in tissues and local capture by tumor cells by attaching to CD44 receptors (Choi et al 2012). Therefore, HA might be responsible for prolonged localization of gold atoms in the tumor tissue providing their gradual distribution. Such an approach can be used both in diagnosis and therapy of malignant tumors.

We suggest that high molecular HA-melanin-based GNPs be used for local application, because of their high viscosity and high affinity to connective tissues, whereas low molecular HA characterized by low viscosity can be used in GNPs for systemic intravenous application.

In the present study we examined the structure, chemical composition and cytotoxicity of HAMG-NPs, as well as their X-ray contrasting properties and their prospective application as a CT contrast agent, using human U251MG cells and the nude mouse flank tumor model.

8. STUDY OBJECTIVES

1. Evaluate optical properties of hyaluronic acid-melanin-based (HAMG) NPs based on light absorption.
2. Determine intracellular localization of HAMG-NPs in tumor cells and their toxicity.
3. Analyze X-ray contrasting properties of hyaluronic acid-melanin-based GNPs.
4. Evaluate dose enhancement after local injection into U251MG animal model.

9. MATERIALS AND METHODS

9.1 HAMG-NPs

Colloidal solutions of hyaluronic-acid-melanin-based GNPs containing 5000 ppm of gold were obtained from the International research center "Martinex", Moscow, Russian Federation. The particles were produced by a solid-state synthesis and modification of polysaccharide-based polymers. The light absorption was estimated on a UV-2501 PC® optical analyzer (Shimadzu Co. Ltd., Japan). Size and localization of GNPs in U251MG cells were studied using the BioZero® BZ-8000 optical system (Keyence, IL, USA) and the JEM-1400 transmission electron microscope (JEOL Ltd., Tokyo, Japan). The particles were maintained in sterile tubes at 4°C.

9.2 U251MG cell line

Human U87MG cells were obtained from ATCC and cultured at 37°C in a humidified atmosphere of 5% CO2 in MEM (M4655, Sigma-Aldrich, MO, USA) supplemented with 10% fetal bovine serum (FBS; JRH Nichirei Biosciences, Tokyo, Japan) and 1% penicillin-streptomycin (100 U/ml penicillin, 0.1 mg/ml streptomycin, Sigma-Aldrich, MO, USA).

9.3 U251MG animal model

The flank tumor model was obtained by a subcutaneous injection of $5x10^6$ U251MG cells in the left thigh of Balb/C nude mice. The cells were suspended in 0.05 ml of equal volumes of MEM and Matrigel. The tumor volume was estimated as a half of the small diameter squared times the large diameter. Tumors over 100 mm^3 were defined as eligible for the local GNPs injection. The use of animals was approved by the ethical committee.

9.4 Cytotoxicity assay

The cytotoxicity analysis was performed to show the cell proliferation after incubation with GNPs and to determine the maximum gold concentration in the medium applicable for the experiments. 100 µl of MEM with 8000 of U251MG cells was placed in each well of 96-well plates and incubated for 24 h. The medium was replaced by MEM with HAMG-NPs or HA-Au (Au^{+3}) (15 - 150 µg gold/ml) and further incubated for 24 h. The medium was removed and the cells were washed twice with PBS. 2 ml of 3-(4,5-dimethylthiazol-2-yl)-5-(3-carboxymethoxyphenyl)-2-(4-sulfophenyl)-2H-tetrazolium (MTS) solution with PMS (Cell Titer 96® AQueous One Solution, Promega, USA) were mixed with 10 ml of MEM, and added in the amount of 100 µl to each well. The cells without GNPs were used as controls. The plates were incubated and the absorption at 490 nm was assessed using a Mithras LB 940 Multimode reader (Berthold Technologies, Germany) after 2 h. The wells containing cells with GNPs without MTS solution were used as additional controls.

9.5 CT scan

The X-ray CT scan was performed using a Latheta LCT-100 Lite (Hitachi Aloka Medical, Ltd., Japan) CT scanner for small animals, operated at 50kVp. The mice were anaesthetized with phenobarbital sodium, 30 mg/kg of body weight. GNPs were injected into the tumor tissue in the volume of 50 µl in each of 2 – 3 injections from different sides of the tumor. The CT scan was performed before the injection, right after the injection and 6 hours after the injection of GNPs.

9.6 Transmission electron microscopy

The JEM-1400 transmission electron microscope (JEOL Ltd., Tokyo, Japan) operated at an accelerating voltage of 120 kV was used to analyze the size and localization of GNPs in U251MG cells in vitro and the presence and location of GNPs in the tumor tissue in vivo. In the experiment in vitro, U251MG cells were incubated with HAMG-GNPs at a gold concentration of 15 μg/ml during 24 h. After incubation, cells containing nanoparticles were washed twice with PBS, centrifuged, fixed and submitted for further processing. In the experiments in vivo, animals were anaesthetized and sacrificed, the tumor tissue obtained after the CT scan was cut, fixed and submitted for further processing. Samples were mounted on copper grids and placed into the TEM. GNPs size and intracellular localization were analyzed using TEM images.

9.7 Radiation treatment

Mice in the "irradiation" and the "GNPs+irradiation" groups were anaesthetized with phenobarbital sodium (30 mg/kg of body weight) and placed onto a special mouse holder plate for the Hitachi MBR-1520R biological X-ray irradiator. Mice bodies were shielded with lead except for the tumor region; the plate was placed into the irradiator at a distance of 350 mm from the X-ray tube. The dose of 8 Gy was delivered to the tumor region with the irradiator operated at 150 kV and 20 mA.

9.8 Statistical analysis

The cytotoxicity experiments were repeated at least 3 times each. The cytotoxicity and tumor growth data represent means ± SDs, p-values were calculated by one-way ANOVA.

10. RESULTS AND DISCUSSION

10.1 Light absorption by HAMG-NPs

Optical properties of HAMG-NPs in the colloidal solution obtained from International Research Center "Martinex" were studied to verify the presence of nano-sized particles and their stability in the solution before using them in experiments on cells and animals. Normalized light absorption spectrum HAMG-NPs colloidal solution is presented in Figure 12. Similarly to the previously studied 8 and 50 nm oligoglycine-coated GNPs, the formation of the absorption peak is determined by the plasmon resonance (Bohren and Huffman 1983, Kreibig and Vollmer 1995). The single peak at 526nm confirmed the presence of nano-sized particles and showed the stability of the colloidal solution. The narrow peak represented more uniform particle size distribution.

10.2 Localization of HAMG-NPs in tumor cells in vitro

Transmission electron microscopy revealed the localization of HAMG-GNPs in U251MG cells in vitro (Figure 13). On TEM images HAMG-NPs were clustered in vacuoles and localized in the cytoplasm of glioma cells without obvious nuclei penetration, similarly to the previously studied oligoglycine-based 8 and 50 nm GNPs. The location of particles in close proximity to the cell nuclei may play a role in the DNA damage by secondary photons and electrons. Free radicals in this case may play a role in the oxidation of lipids and further destruction of membrane structures of tumor cells.

10.3 Composition and cytotoxicity of GNPs

The biocompatibility of GNPs may play the main role in the selection of certain types of particles to be used in living organisms. Spherical nanoparticles may show

better biocompatibility, than other structures, because of their form and the uniform outer layer of the stabilizing agent, though certain peculiarities of particle composition may increase their toxicity. As mentioned earlier, the toxicity may be connected with the amount of ionized gold in the outer layer of the spherical particles. In our study, we compared the cytotoxicity of HAMG-NPs with the HA-Gold (Au^{3+}) solution (Figure 14). The MTS assay showed a very high toxicity of the ionized gold, and relatively non-toxic nanoparticles, where gold is covered by the layer of HA and the layer of melanin, which stabilized the ionized gold to the 0-valency (Figure 11).

HAMG-NPs were non-toxic within the studied gold concentration range (15 to 150 μg/ml), though local and intravenous injections of the same nanoparticle may have a different effect on the animal organism.

In the present study we examined the effects of gold nanoparticles only on tumor cells, though the comparison with normal cells would give better understanding of further applicability of gold nanoparticles in biological systems, such as animal tumor models, and further studies are required to evaluate such applications.

10.4 X-ray contrasting properties of HAMG-NPs

CT scans showed no contrast in the tumor areas before GNPs injection, and contrasting of the tumor area right after and 6 h after the injection (Figure 15). The character of the contrasting determined the possibility to distinguish the tumor tissue from the normal tissue, and showed that the particles could be redistributed within the tumor tissue after 6 hours, without being washed out by blood. The CT-scanner was operated at 50 kVp. In our consideration, this energy might better comply with the X-ray absorption by Iodine-containing contrast agents, and the use of energies closer to the

inner atomic orbit edges of gold atoms might help to achieve more significant photon absorption and better contrasting on CT images.

10.5 Glioma radiosensitization

The tumor growth rate in animals with/without treatment using GNPs and radiation is shown in Figure 16. The difference between “radiation” and “gold+radiation” groups was not statistically significant, though there was a tendency of faster tumor growth in mice irradiated without gold nanoparticles. There were several reasons for this. U251 malignant glioma showed very slow growth in the current experiment, which could influence the results. 2 mice died in the radiation group in the middle of the experiment, and the statistical significance decreased. The irradiation with 8 Gy might not be enough to interact with tumor cells and gold nanoparticles, and higher doses might have a better effect. Local injection of gold might lead to an inhomogeneous distribution in the tumor mass and decrease the effect of radiosensitization with gold. The flank tumor model might not represent the state of events with the real brain tumor. In future studies we should consider these factors to increase the statistical significance. We can use a different tumor mode, intravenous injection of gold nanoparticles, a larger population and different irradiation doses.

Concerning radiation enhancement properties, gold is an expensive material and is not the only candidate. In this regard, different materials were tested for tumor radiosensitization. Among them nicotinamide plus carbogen (Nishioka et al., 1999), 1-(1′,3′,4′-trihydroxy-2′-butoxy) methyl- 2-nitroimidazole (RP-343), RP-170, etanidazole (Murayama et al., 1993); 1-(2′-oxopropyl)-5-fluorouracil (OFU001) (Shibamoto et al., 2001). A CT contrast agent containing iodine (Z=53) (Adam et al., 2006) was also tested for radiosensitization. MRI contrast agents with gadolinium (Z=64) were

similarly suggested for radiosensitization. Nevertheless, the potential effect of higher-Z materials such as gold was predicted to be more significant than that of other chemical compounds (Hainfeld et al., 2008). We believe that further studies in this area might help find a cheaper radiosensitizer with properties close to those of gold nanoparticles.

In our study we used a keV-radiation source for in vitro and in vivo experiments, though in clinical practice MeV-energies are applied to the patients with malignant gliomas. According to the literature data, the use of a 6MV X-ray irradiator could provide the radiosensitization of breast cancer MDA-MB-231 cells with gold nanoparticles with a dose-enhancement factor of 1.29 ($p=0.002$), the study showed cell-specific radiosensitization (Jain et al., 2011). The effect of high-energy X-rays can be explained by the production of a large number of scattered photons, when MeV-X-rays interact with gold nanoparticle. In this process, initial photons possess much higher energy than photons in the keV-range observed in the current study. Thus, they can interact with several gold atoms, losing their energy and changing direction in the matter and producing larger number of secondary photons and electrons. As photons lose part of their energy after collision with gold atoms, they can continue their pathways in the tissue with energy lower than the MeV-range, e.g. keV-energy, producing similar effects as described in the current study. Therefore, we suggest that using MeV photons with gold nanoparticles may have prospects in future experiments and clinical application.

Proton radiotherapy may also have potential in the treatment of glioma with gold nanoparticle radiosensitization. As was shown by Kim et al. (2010), high-Z particles can emit secondary photons and increase the absorption dose after proton irradiation (Kim et al., 2010). Similarly to MeV X-rays, protons possess MV energy and can interact with high-Z materials. Protons are much bigger than electrons and may collide with

several electrons in several gold atoms along their pathway in matter, producing a large number of secondary electrons and photons, leading to tumor cell DNA or membrane damage. As protons irradiate mainly the area of the main tumor mass if the Bragg's peak is focused on the tumor, other tissues are irradiated in smaller doses, even if they contain nanoparticles. Therefore, proton radiation combined with radiosensitization using gold nanoparticles may have advantages in comparison with conventional X-ray radiotherapy, though further studies are required to evaluate the efficacy of this method.

10.6 Pathological analysis

On light microscopy and TEM images of the samples of tumor tissue from the animal model, GNPs appeared to be clustered in vacuoles as in U251MG cells 6 h after the injection similarly to the in vitro experiments, showing the potential for X-ray radiosensitization (Figure 17). GNPs were clearly seen in the tumor cells between the muscle fibers after three injections in one week (Figure 18). In this case, the particles could be transferred by blood within the tumor tissue and selectively captured by tumor cells. Presence of GNPs within the tumor cells in vivo might be related to the properties of HA to attach to the tumor cell CD44 and other receptors and be captured into the cytoplasm, though these mechanisms are yet to be clarified.

10.7 GNPs delivery to the tumor cells in vivo

In this study, we suggest that the particle composition and especially hyaluronic acid played a role in the selective and prolonged accumulation of HAMG-NPs in glioma cells in vivo. Concerning the delivery of particles to the tumor cells, a number of methods and drug-delivery systems have been studied in recent years. One of the methods involves the use of liposome carriers to deliver gold nanoparticles to the tumor cells. Liposomes are presented as 80–100 nm spherical structures of bilipid membranes

which surround the active compounds inside them. Gold nanoparticles may be incorporated into liposomes with active molecules, such as polysaccharides or antibodies, or both. Liposomes may easily penetrate tumor tissue capillaries because of the enhanced permeability and retention (ERP) effect, though smaller single nanoparticles may have better penetration abilities. Gold nanoparticles can be functionalized similarly to polysaccharides or antibodies, or both. The specificity of accumulation of gold nanoparticles in tumor tissues is a challenge for future studies.

11. CONCLUSION

1. HAMG-NPs were present in the stable colloidal solution and showed optical properties typical of nano-sized spherical particles.
2. HAMG-NPs were captured by U251MG cells in vitro, clustered in vacuoles in the cytoplasm of glioma cells, without obvious nuclei penetration.
3. HAMG-NPs provided contrasting of the tumor tissue in vivo right after the injection; later they were redistributed in the tumor and captured by tumor cells, providing the possibility to be used not only as a contrasting agent for X-ray CT but also as radiosensitizers in vivo.
4. Further studies are required to evaluate the biodistribution of HAMG-NPs and their radiosensitization properties in vivo.

12. FUTURE PROSPECTS

Functionalized HAMG-NPs show the ability to be captured by tumor cells in vivo after local injection. Though HA may play the role of an active molecule on the surface of GNPs, the intravenous injection of HAMG-NPs may lead to an excessive load in different organs, such as the liver, where the particles may impair the normal function. Although the EPR effect contributes to the diffusion of macromolecules and ultrafine materials into the tumor tissue through leaky tumor vessels and within the tissues (Dvorak et al 1988, Maeda et al 2000, Furuyama et al 2009), further development of functionalization considers more advanced properties of nanoparticles, when, after the targeted delivery, agents can fix to biological structures with or without transformation and stay within cells during a certain period of time needed for further diagnostic or treatment procedures. The attachment of polysaccharides or antibodies to the particles directly or to the outer layer of the particle carriers, e.g. liposomes, was found to be effective in achieving higher functionality (Chithrani et al 2010, Liu et al 2010, Jiao et al 2011, Kumar et al 2012). Also, such functionality was recently demonstrated in studies with targeted GNPs used as X-ray and CT contrast agents (Popovtzer et al 2008, Aydogan et al 2010, Reuveni et al 2011).

Further development of functionalization with the attachment of active molecules, such as complex polysaccharides or antibodies, and targeted delivery of GNPs, either individually or incorporated in specific carriers such as liposomes, may lead to more advanced diagnostic and therapeutic applications of the nanoparticles, not only in fundamental research, but also in clinical trials in future.

FIGURES AND TABLES

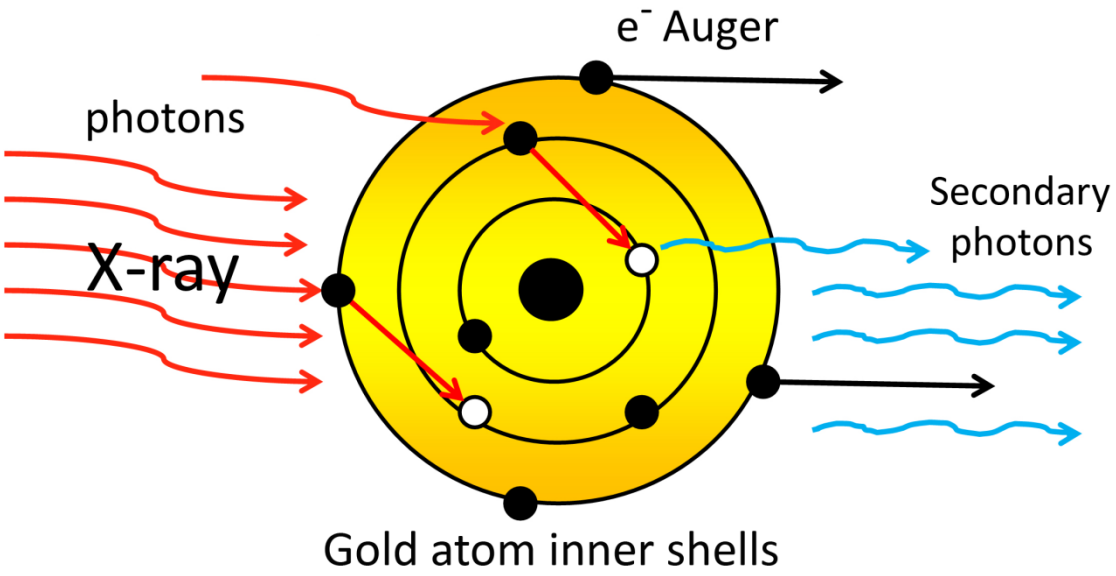

Figure 1 Interaction of X-rays with electrons at the inner glod atomic orbits (schematically). Irradiated by photons of a certain energy range gold can emit additional photons and electrons. Initial photons knock out electrons at the inner K, L and M gold atomic orbits, the vacant places of the missing electrons are occupied by electrons from the higher orbits, and the difference in energy is emitted as secondary (fluorescent) photons, accompanied by ejected Auger electrons.

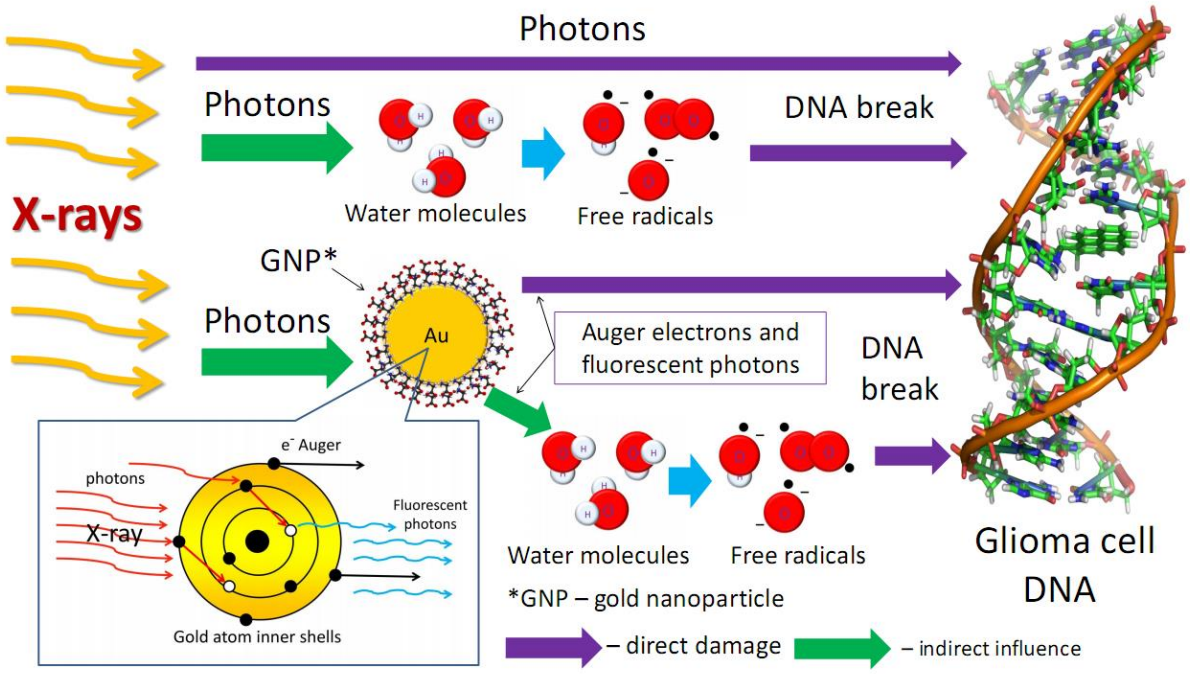

Figure 2 Direct and indirect damage of tumor cell DNA. Initial X-rays damage tumor cell DNA and other components through the direct influence of photons and indirect influence of free radicals, formed in the water medium. GNPs capture X-ray photons and emit photons and electrons, producing similar direct and indirect damage to the DNA and other cell components. DNA damage is mainly caused by HO* radicals, though low energy electrons and prehydrated electrons may also be invovlved (Chatterjee and Magee 1985, Boudaiffa et al 2000, Sanche 2002 and 2009, Brun et al 2009, Wang et al 2009, Han et al 2010). Sample DNA helix was designed using Pymol software (www.pymol.org) from the 2L8Q code (Julien et al 2011).

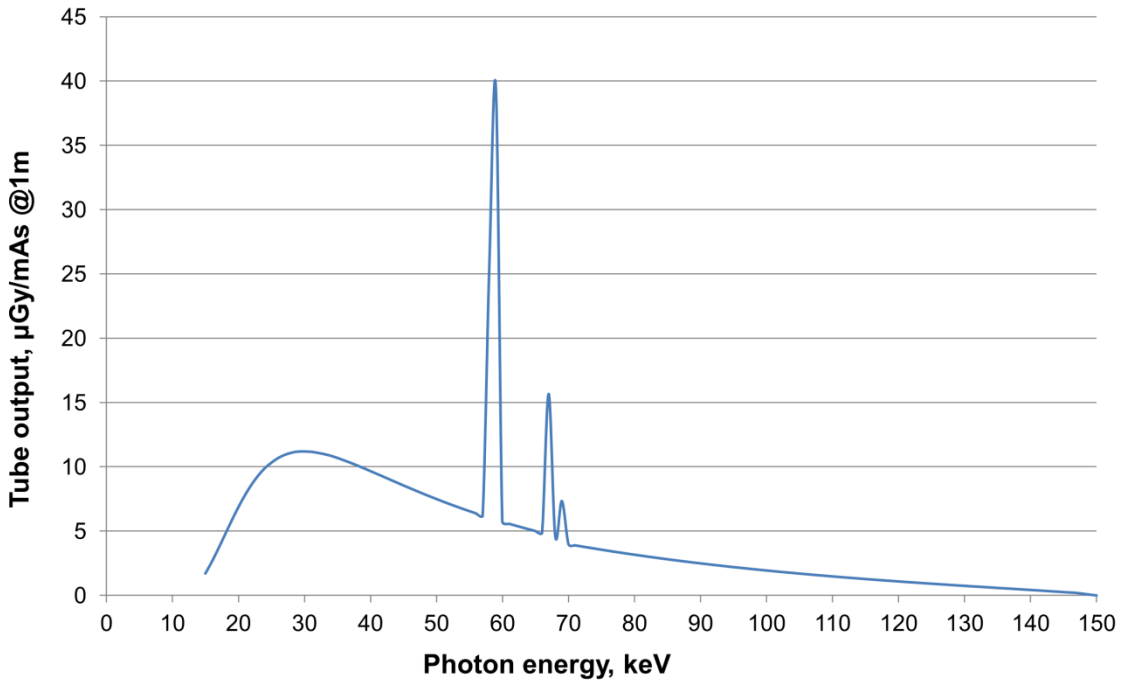

Figure 3 The Hitachi MBR-1520 biological irradiator spectrum. Calculation was made using SpekCalc® software (Poludniowski et at 2007, 2009). The spectrum includes energies over K- (68.0–80.7 keV), L- (11.9-14.4 keV) and M-edges (2.2–3.4 keV) of gold atoms, necessary to eject electrons from the inner shells, though the resonant influence on the M-shell might not be significant.

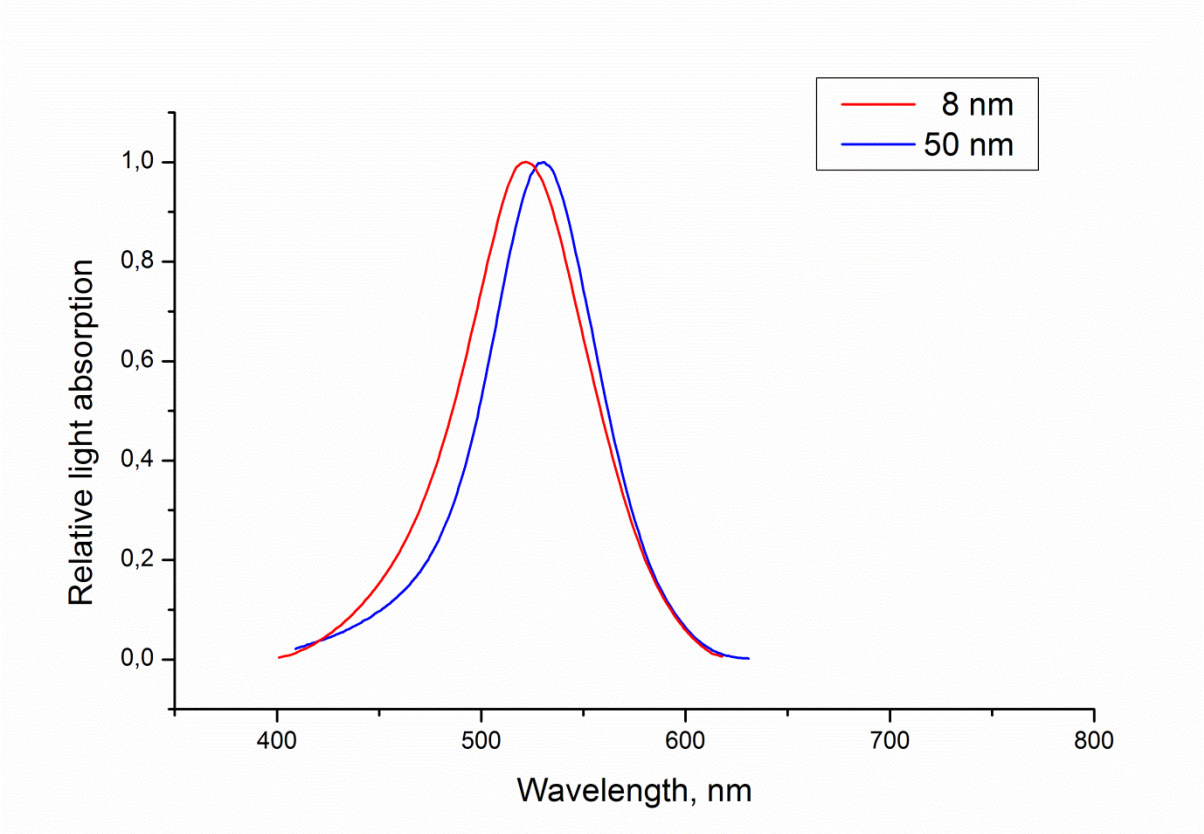

Figure 4 Light absorption by 8 and 50 nm GNPs. Distinguished peaks for each particle type at different wavelengths confirm the presence of nano-scaled particles and show the stability of the the colloidal solution. The narrower peak of 50 nm GNPs represents more uniform particle size distribution.

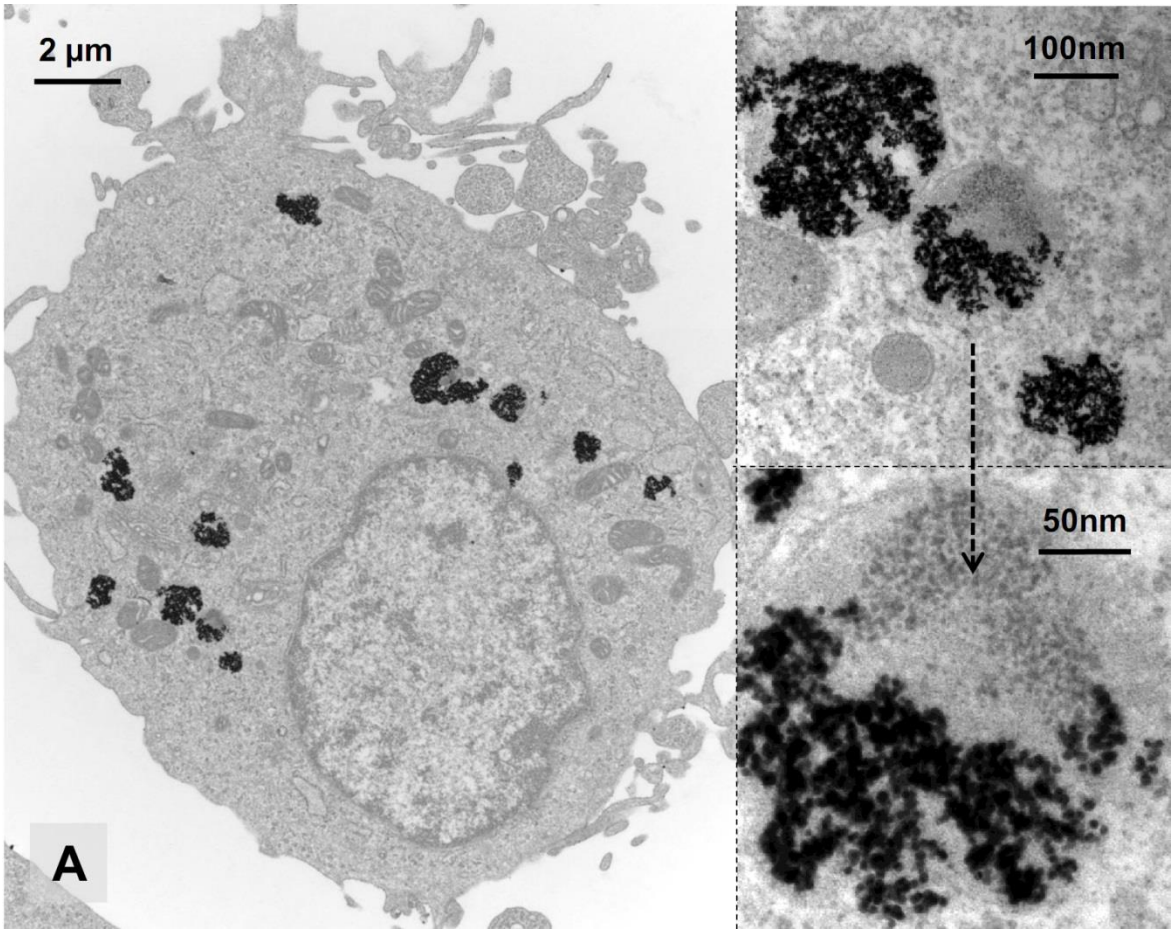

Figure 5A Transmission electron microscopy: the localization of 8 nm GNPs in U251MG cells. GNPs are clustered in vacuoles and localized in the cell cytoplasm without obvious nucleus penetration. Gold concentration - 15 µg/ml, 24 h incubation.

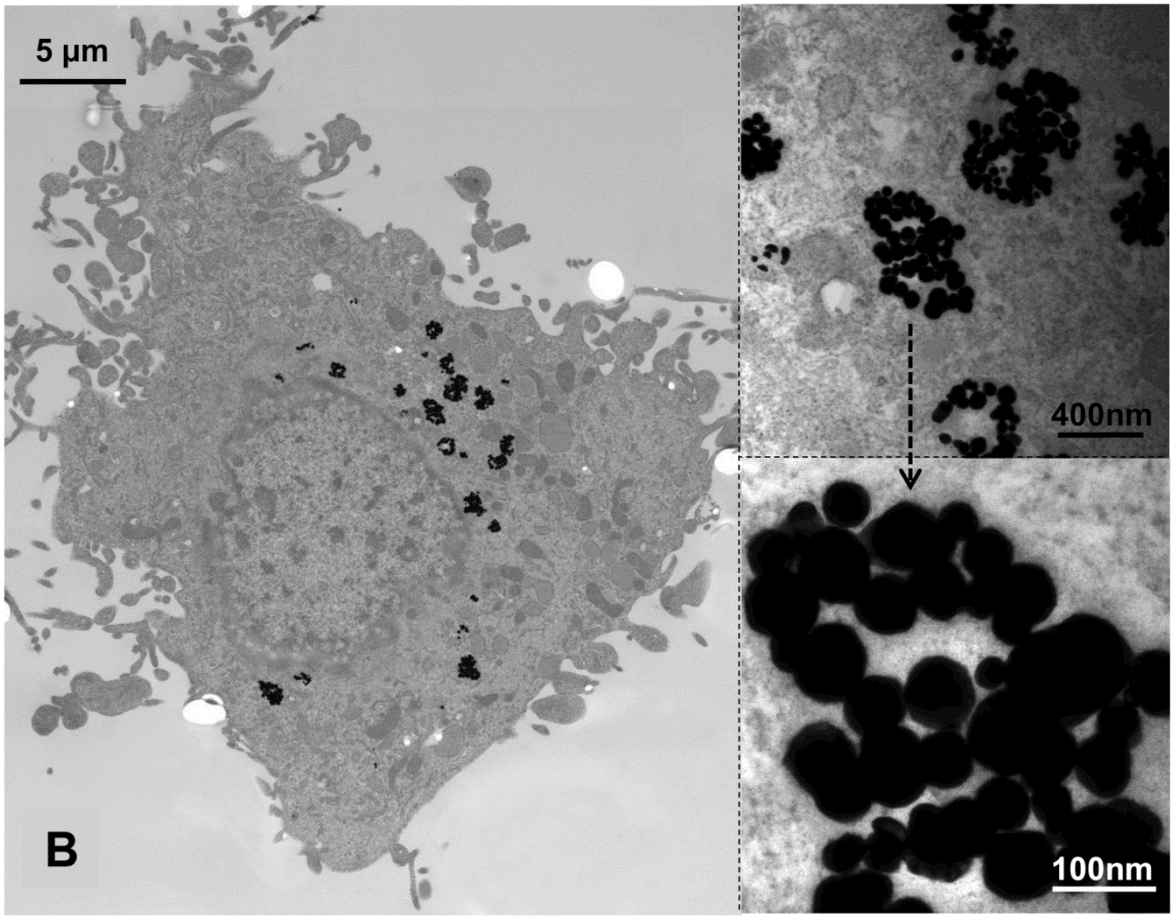

Figure 5B Transmission electron microscopy: the localization of 8 nm GNPs in U251MG cells. GNPs are clustered in vacuoles and localized in the cell cytoplasm without obvious nucleus penetration. Gold concentration - 15 µg/ml, 24 h incubation.

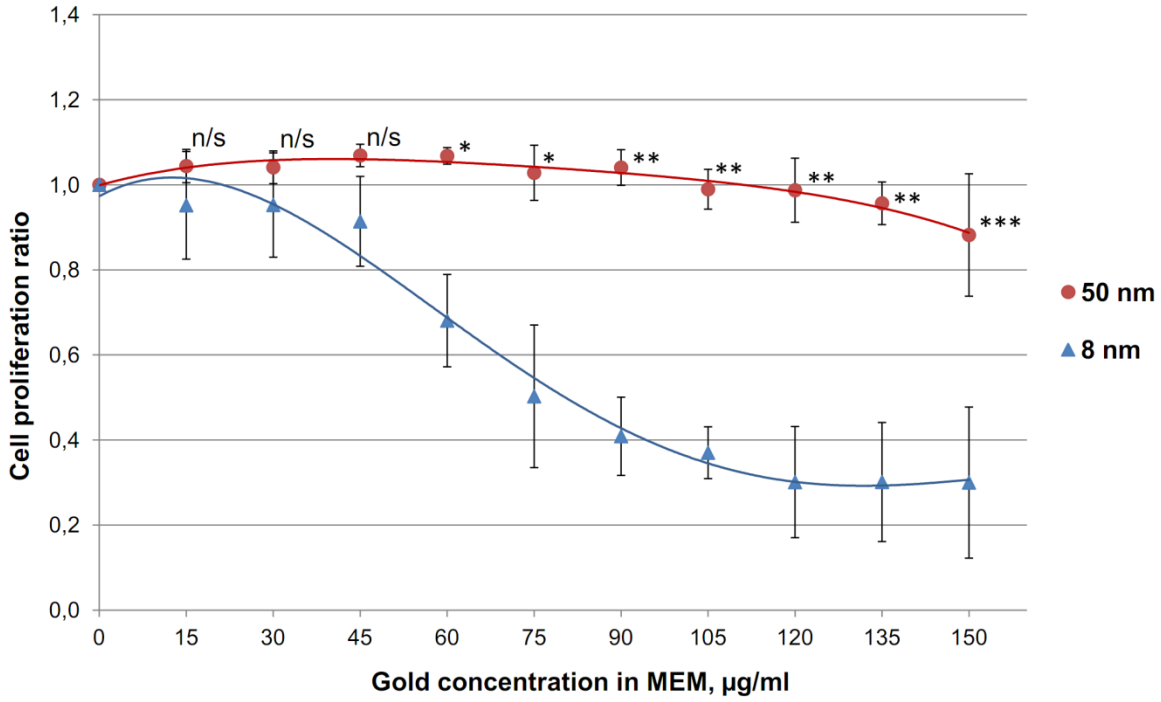

Figure 6 The concentration- and size-dependent cytotoxicity of GNPs for U251MG cells. The cytotoxicity is shown as a ratio of GNPs-containing cell proliferation to the controls without GNPs, where the proliferation equals 1 (or 100%), (*$p<0.01$; **$p\leq0.002$; ***$p=0.012$). The data represent means ± SDs, p-values by one-way ANOVA.

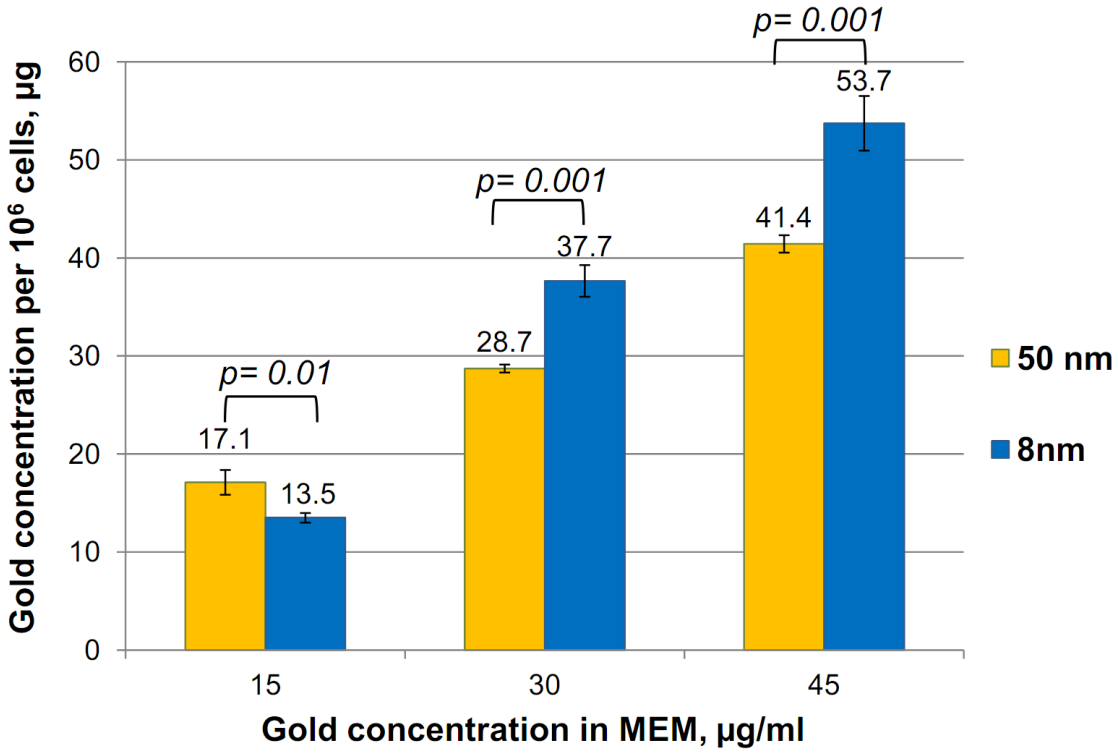

Figure 7 Concentration-dependent gold accumulation in U251MG cells. The accumulation is shown as the amount of gold (µg) in 10^6 cells after 24h incubation. The data represent means ± SDs, p-values by one-way ANOVA.

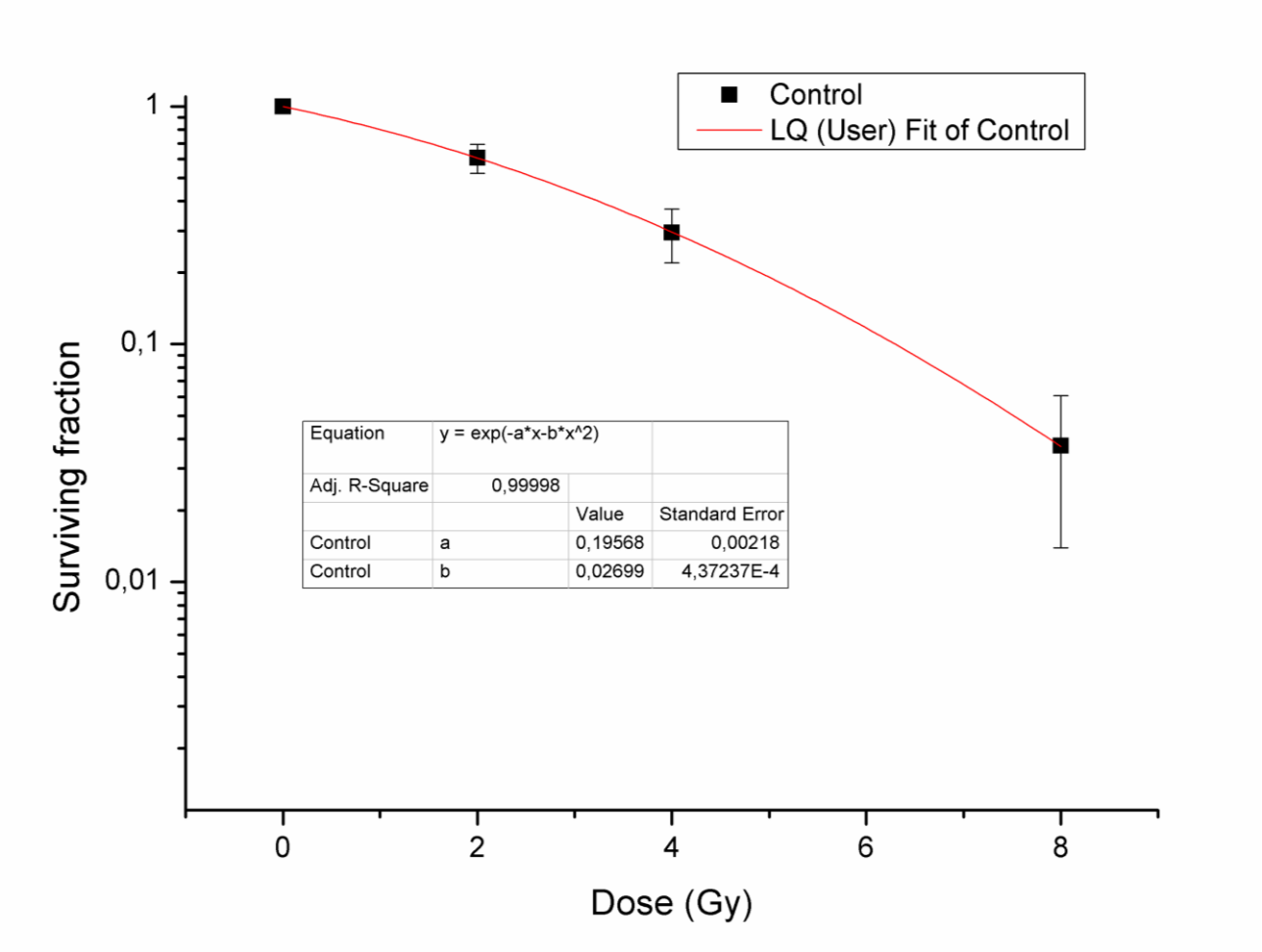

Figure 8 The U251MG cells survival curve (control) fitted to the linear quadratic model. The linear parameter α and the quadratic parameter β were obtained from the curve fit according to the linear–quadratic formula formula $SF = e^{-(\alpha D+\beta D^2)}$, where D is the irradiation dose (x in the equation on the graph). The accuracy of the fit is represented by the R^2=0.99998.

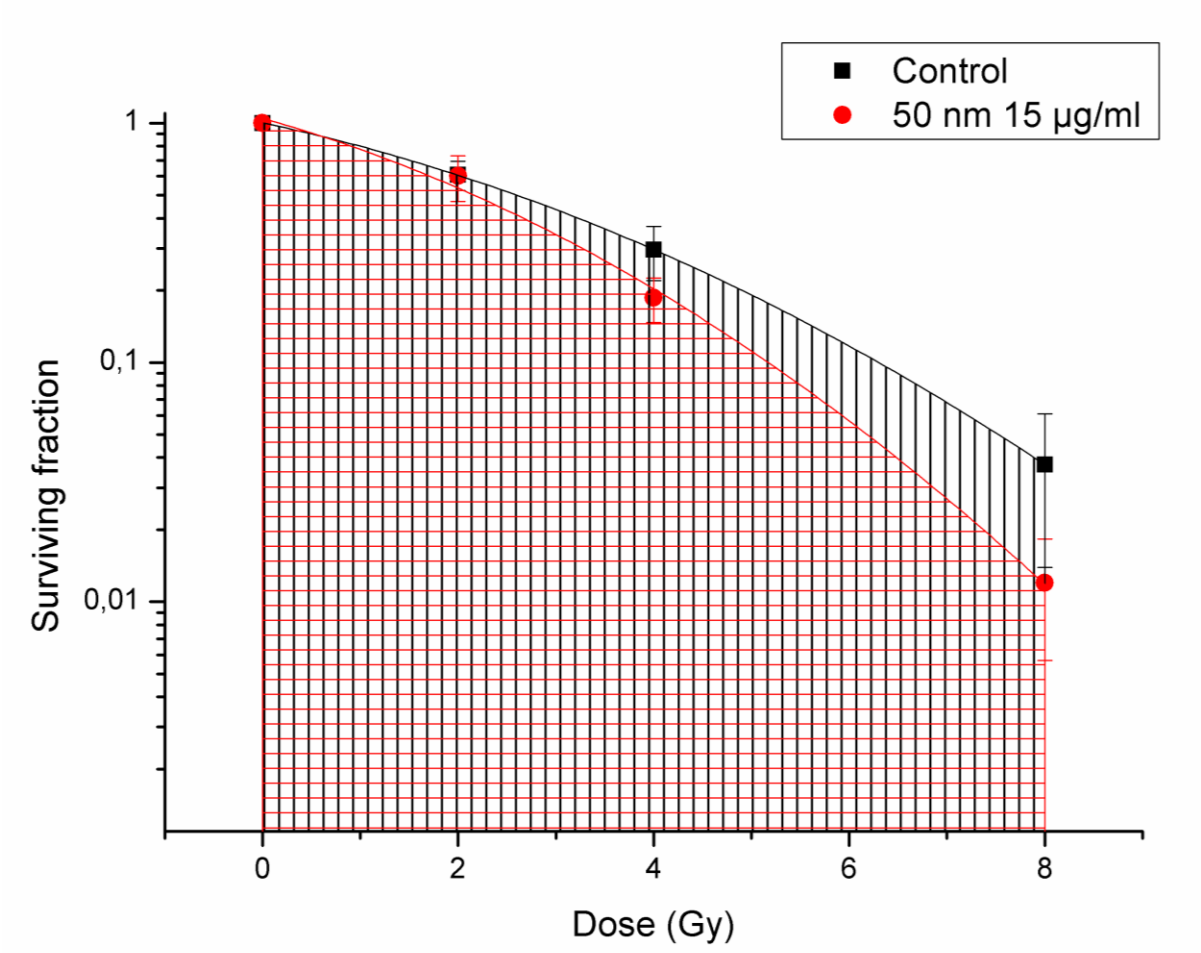

Figure 9 AUC (area under curve) - the area under the fitted LQ model curves. Calculated to determine the statistical significance between the treatment curves and the controls as a definite integral of the linear quadratic function: $AUC = \int_0^8 \exp(-\alpha x - \beta x^2) dx$.

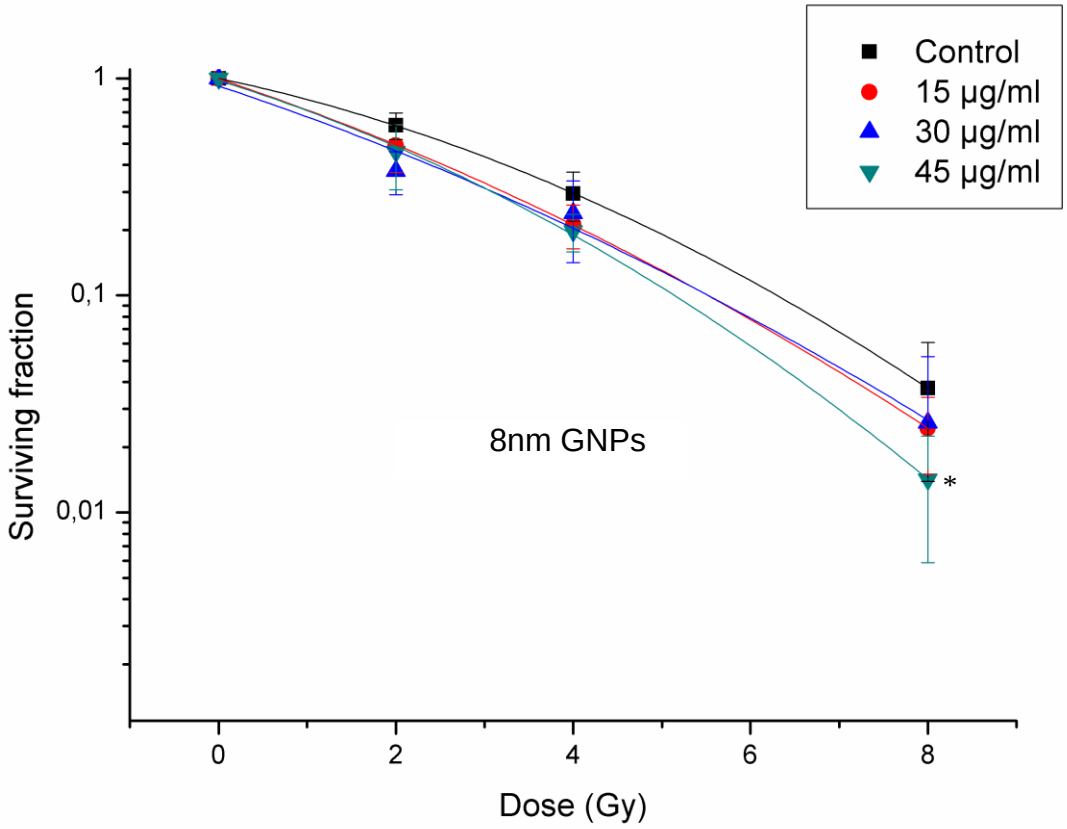

Figure 10A Survival curves of U251MG cells irradiated with 8 nm GNPs. Irradiation with 2, 4 and 8 Gy X-rays after 24 hours incubation with 15, 30 and 45 µg/ml of 8 nm GNPs, compared to the control. At 8 Gy the difference was found significant at 45 µg/ml (*p=0.024). The data represent means ± SDs, p-values by one-way ANOVA.

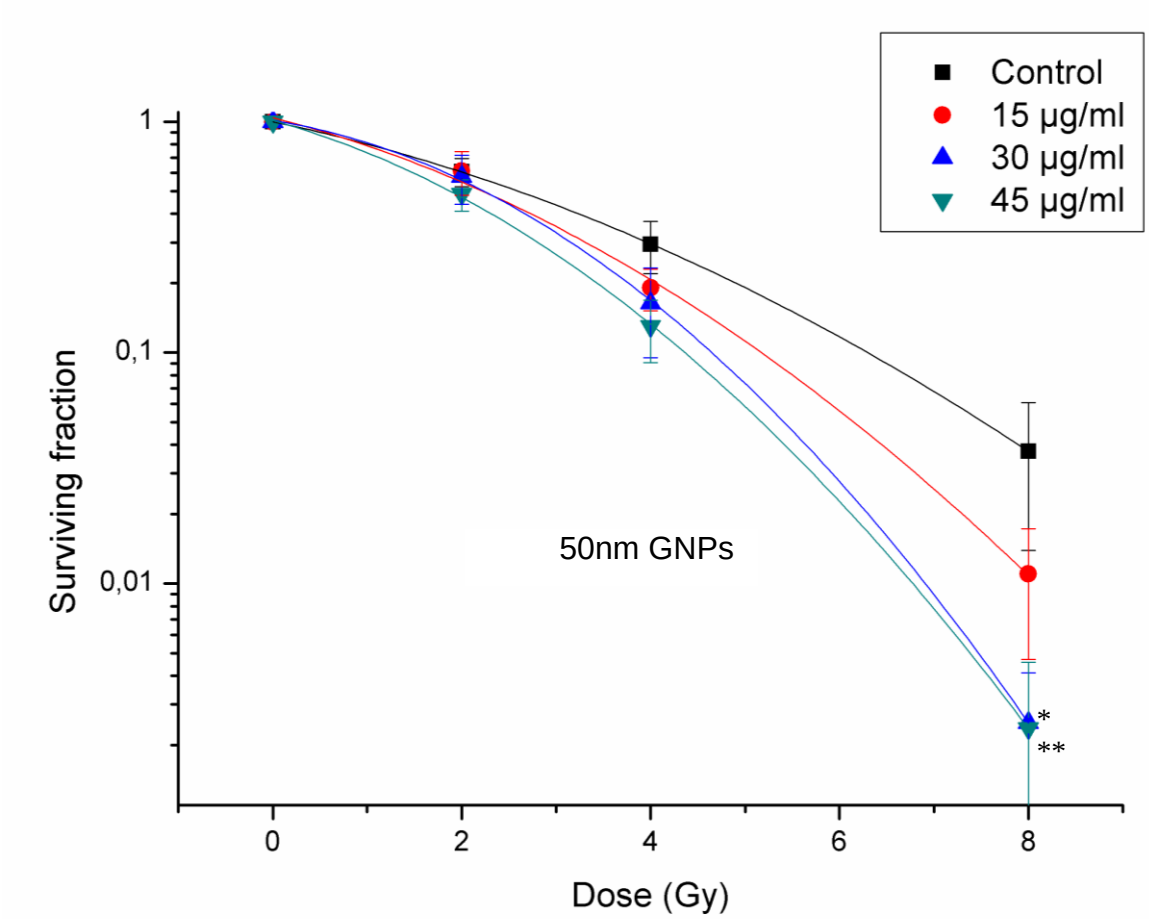

Figure 10B Survival curves of U251MG cells irradiated with 8 nm GNPs. Irradiation with 2, 4 and 8 Gy X-rays after 24 hours incubation with 15, 30 and 45 µg/ml of 8 nm GNPs, compared to the control. At 8 Gy the difference was found significant at 30 µg/ml (*p=0.006) and 45 µg/ml (**p=0.006).The data represent means ± SDs, p-values by one-way ANOVA.

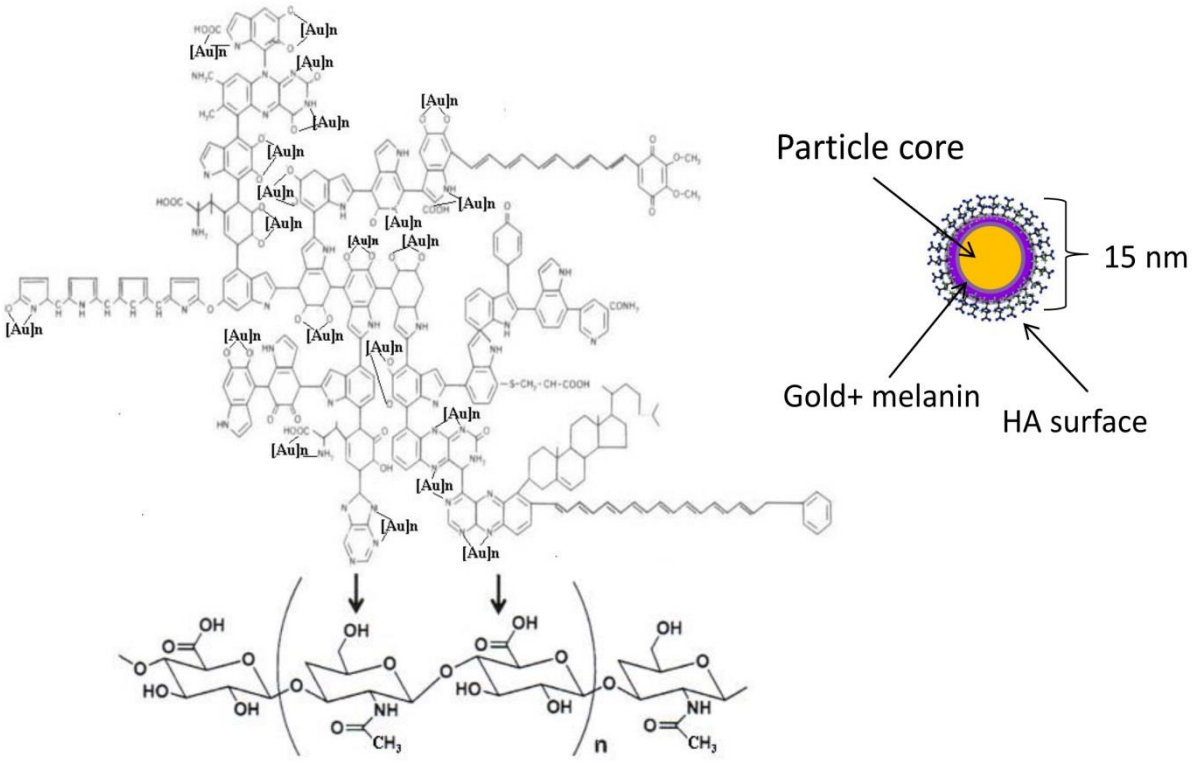

Figure 11 The structure of hyaluronic acid-melanin-based gold nanoparticles (HAMG-NPs). The particles contain melanin (empirical formula $C_{77}H_{98}O_{33}N_{14}S$), a bioactive component stabilizing gold, and modified hyaluronic acid (HA), a matrix carrier for targeted delivery of bioactive compounds.

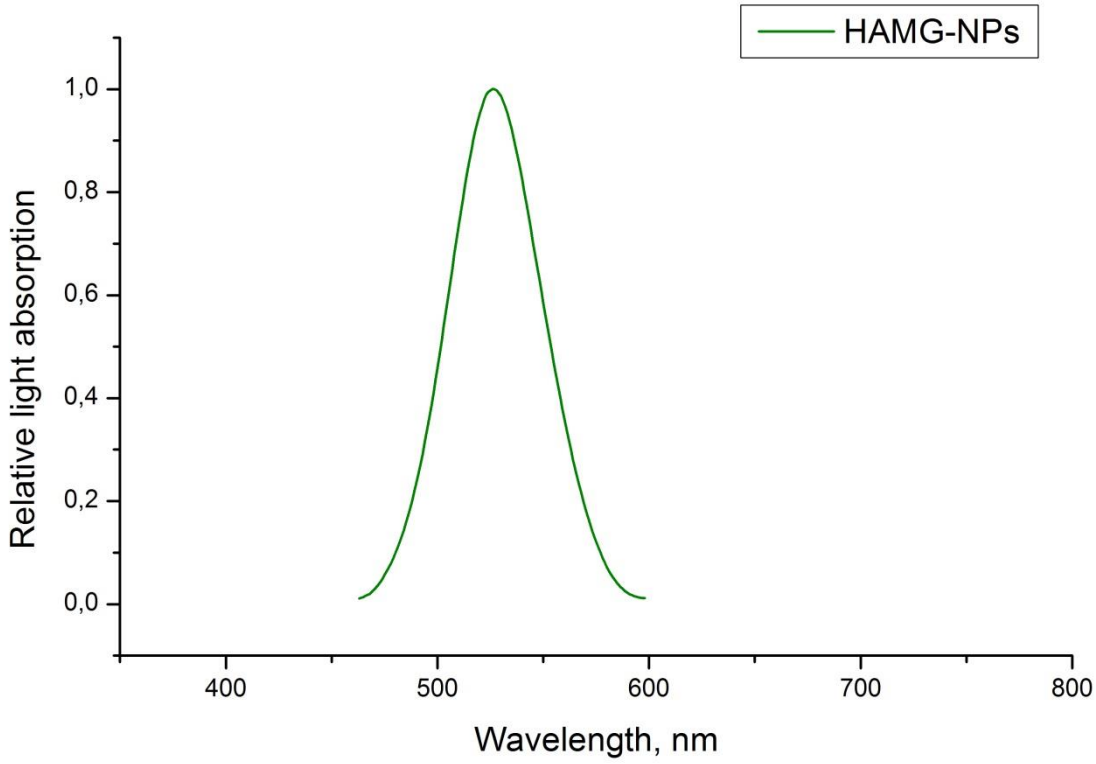

Figure 12 Light absorption by HAMG-NPs. The single peak confirms the presence of nano-sized particles and shows the stability of the the colloidal solution. The narrow peak represents the uniform particle size distribution.

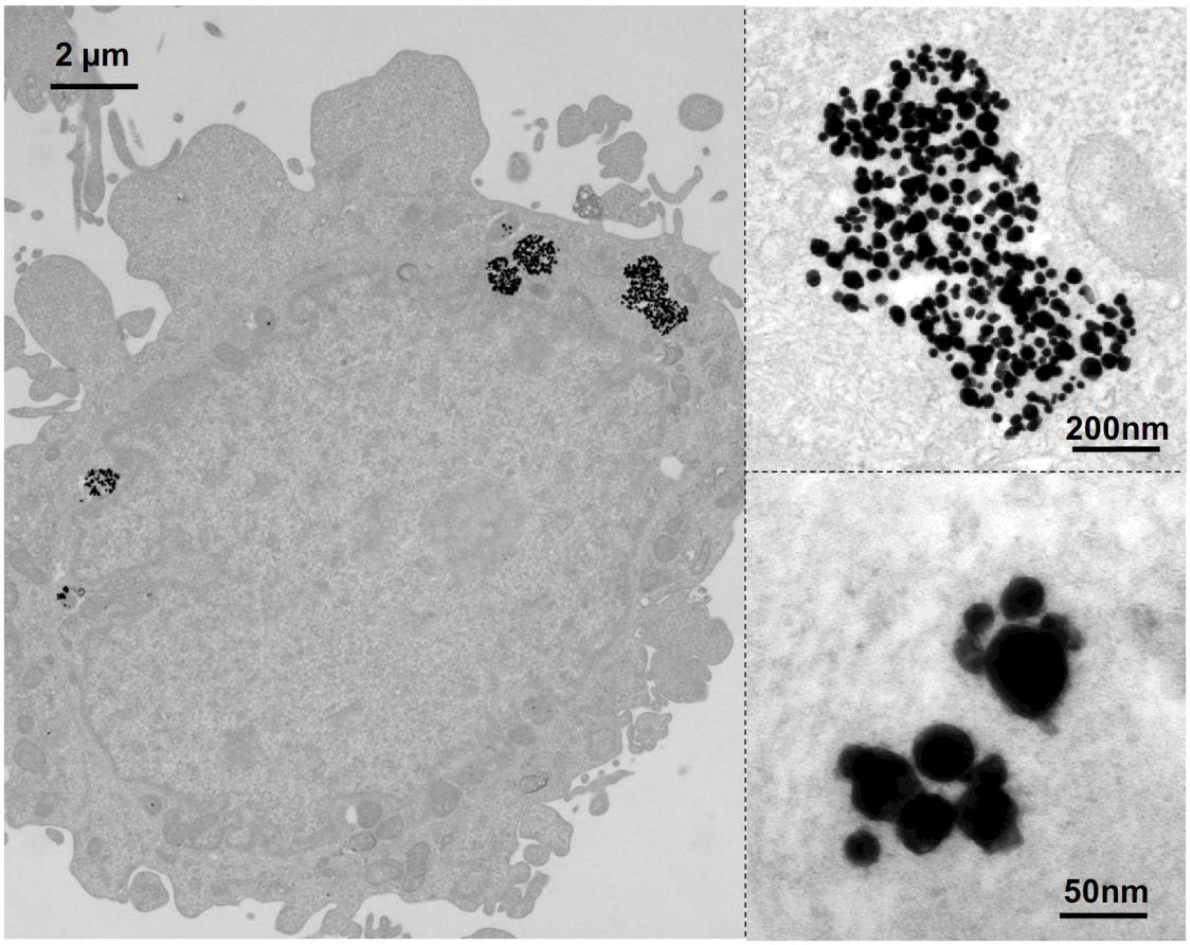

Figure 13 Transmission electron microscopy: the localization of HAMG-GNPs in U251MG cells. GNPs are clustered in vacuoles and localized in the cell cytoplasm without obvious nucleus penetration similarly to the previously studied oligoglycine-based 8 and 50 nm GNPs. Gold concentration - 15 µg/ml, 24 h incubation.

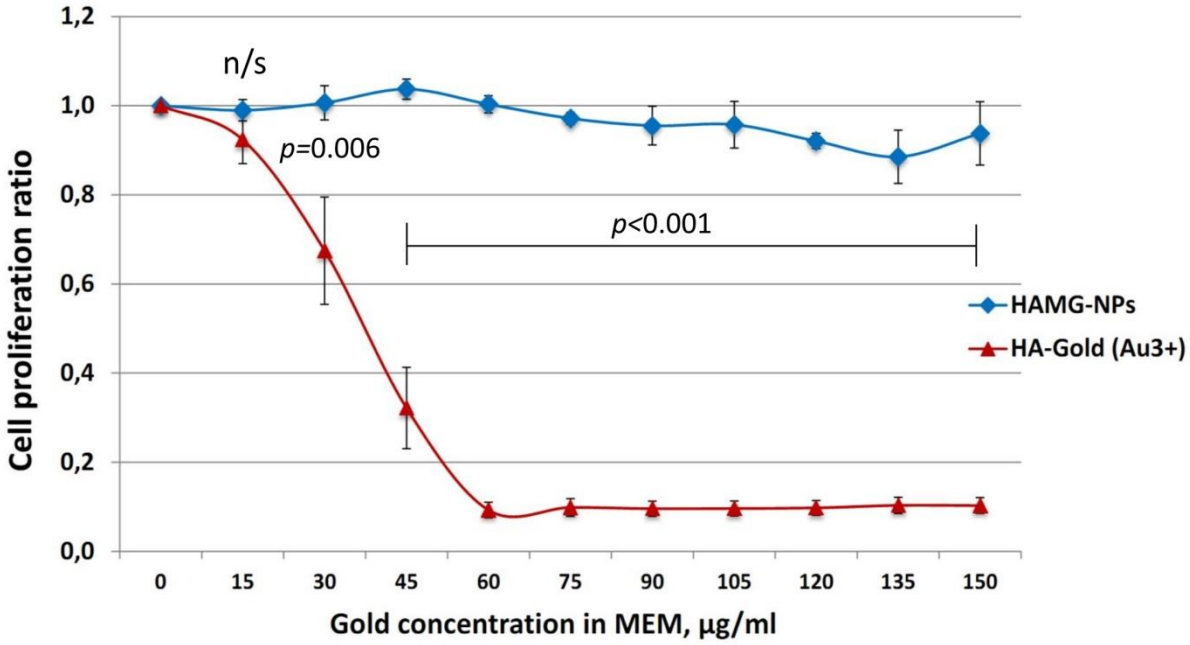

Figure 14 The concentration-dependent cytotoxicity of HAMG-NPs for U251MG cells compared to that of the HA-Gold solution, containinag ionized Au^{3+}. The cytotoxicity is shown as a ratio of GNPs-containing cell proliferation to the controls without GNPs, the control cell proliferation equals 1 (or 100%). The data represent means ± SDs, p-values by one-way ANOVA.

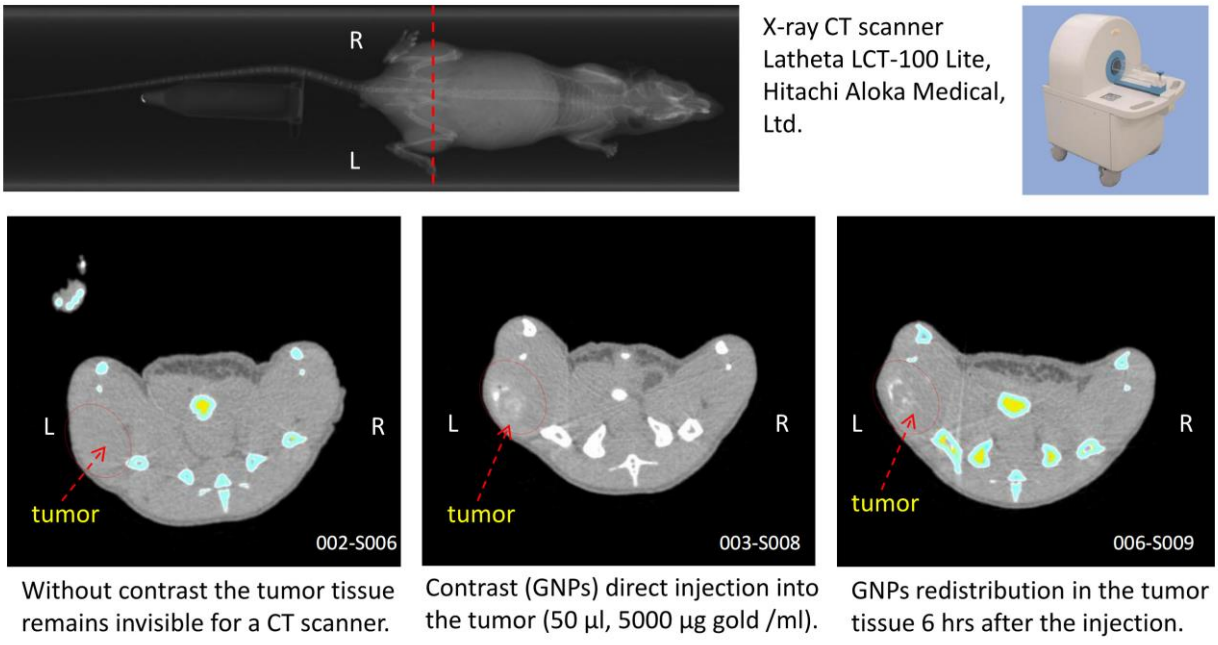

Figure 15 Contrasting properties of HAMG-GNPs. Particles were injected intratumorally into the BalbC nude mice U251MG flank model. Mice were anaesthesized and examined at the Latheta LCT-100 Lite X-ray CT scanner. 6 hours after GNPs injection the contrast distributed within the tumor tissue.

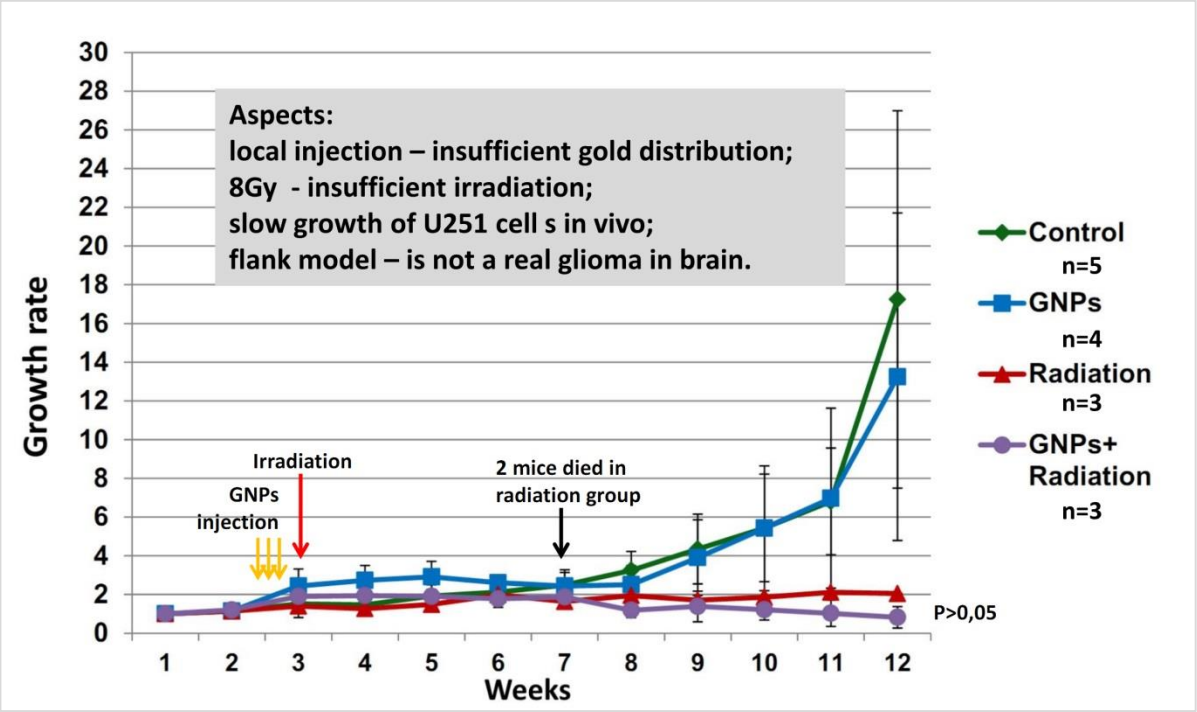

Figure 16 U251MG flank model growth in four studied groups of mice. Stages of experiements and the aspects of the in vivo study are also presented. The tumor growth represent the ratio of the current tumor size to the initial size before the treatment was initiated. The data represent means ± SDs, p-values by one-way ANOVA.

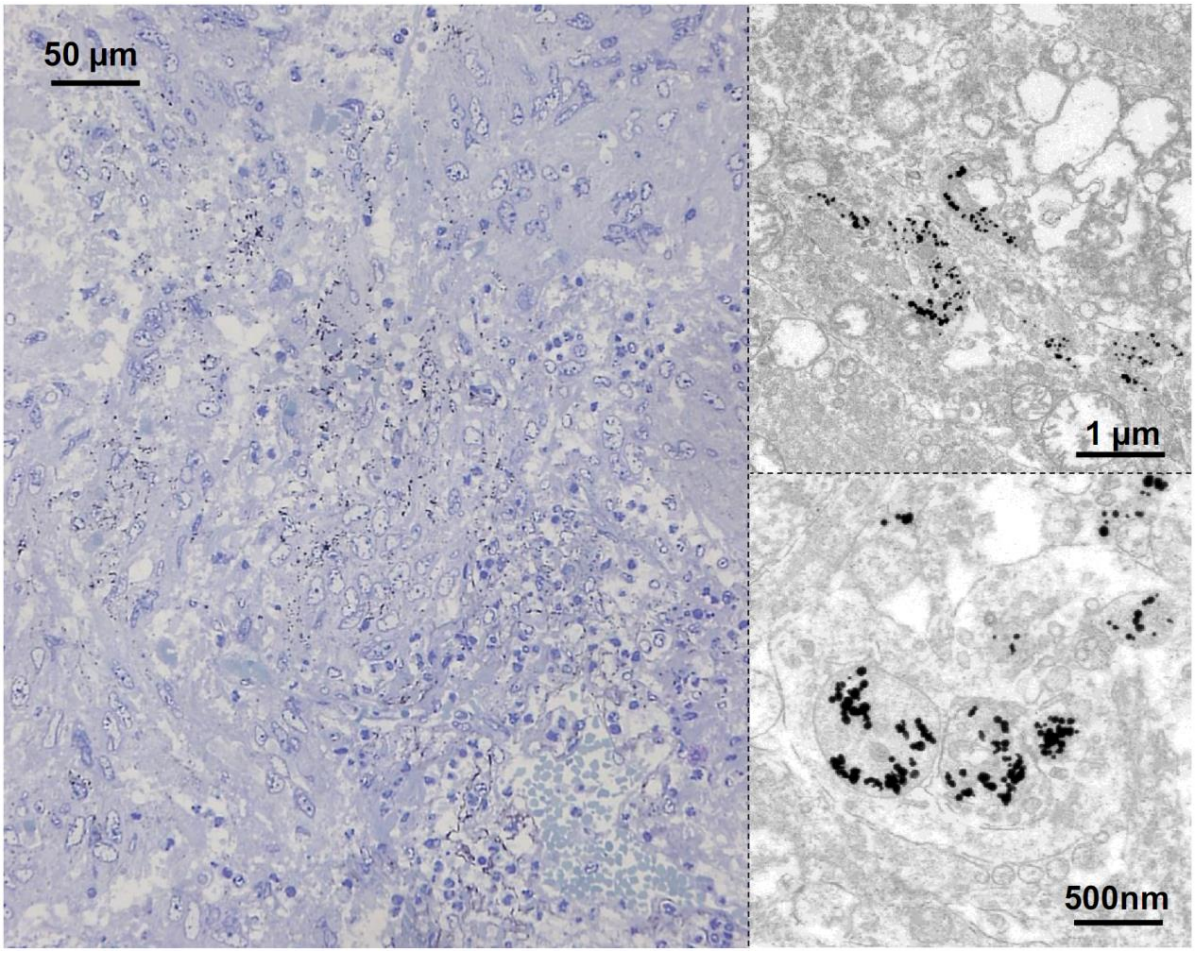

Figure 17 Light microscopy (left) and TEM (right upper and lower) images of U251 malignant tumor cells in the mouse 6 hours after the injection of HAMG-GNPs. GNPs are clustered in vacuoles as in U251MG cells in the experiments in vitro, being eligible for further radiosensitization.

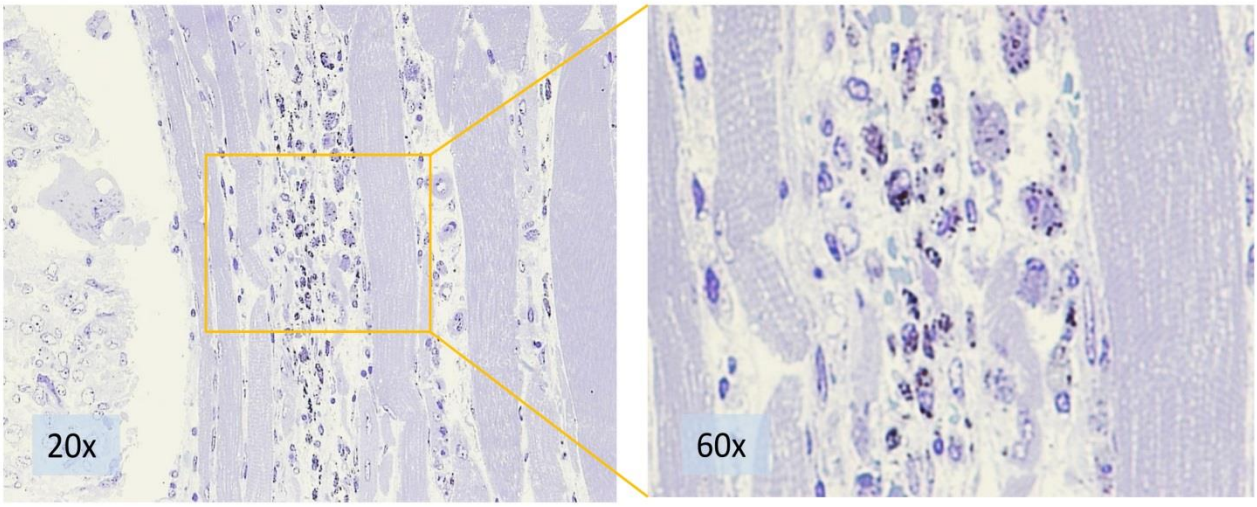

Figure 18 Pathological analysis of the tumor samples after 3 injections of HAMG-NPs and radiotherapy, toluidine blue staining. GNPs are clearly seen in the cell population between the muscle fibers. The muscle fibers are clear from GNPs, showing potential selectivity of hyaluronic acid-coated GNPs.

Parameter		α[Gy^{-1}]	β [Gy^{-2}]	SF_2 dose, Gy	DEF (SF_2)	p-value (SF_2 fit.)	D_{10}	DEF (D_{10})	p-value (D_{10})	AUC	DEF (AUC)	p-value (AUC)
Control		0.196 ±0.002	0.027 ±0.0004	2			6.132 ±0.694			2.897 ±0.431		
8 nm	15 μg/ml	0.314 ±0.002	0.019 ±<0.0001	1.463	1.367	0.208	5.341 ±0.785	1.148	0.081	2.506 ±0.506	1.156	0.169
	30 μg/ml	0.340 ±0.059	0.014 ±0.009	1.391	1.438	0.183	5.659 ±1.031	1.084	0.321	2.560 ±0.526	1.132	0.237
	45 μg/ml	0.306 ±0.017	0.028 ±0.003	1.443	1.386	0.065	5.000 ±0.529	1.226	0.012	2.325 ±0.343	1.246	0.036
50 nm	15 μg/ml	0.191 ±0.033	0.048 ±0.006	1.802	1.110	0.729	5.157 ±0.313	1.189	0.02	2.595 ±0.368	1.116	0.243
	30 μg/ml	0.126 ±0.012	0.079 ±0.003	1.842	1.086	0.294	4.428 ±0.307	1.385	<0.001	2.325 ±0.277	1.246	0.032
	45 μg/ml	0.240 ±0.014	0.066 ±0.003	1.481	1.350	0.082	4.364 ±0.200	1.405	<0.001	2.197 ±0.216	1.319	0.01

Table 1 Summary of radiobiological parameters for U251MG cells irradiated with 150 kVp X-rays with/without GNPs. α and β values derived from fitting the experiment data to the LQ model, $SF=\exp -(\alpha D + \beta D^2)$. SF_2 dose represent the radiation dose for the cells with GNPs needed to obtain the same surviving fraction as 2 Gy irradiation given to the cells without GNPs, DEF (SF_2) in the ratio of SF_2 dose to 2 (Gy). P-values (SF_2 fit.) were calculated from the fitted values of SF_2. D_{10} is the dose needed to achieve 10% of cell survival, and DEF (D_{10}) is the D_{10} ratio between the control and cells with GNPs. AUC is the area under the fitted LQ model curve; DEF (AUC) is the AUC ratio between the control and treatment groups. P-values (SF2 fit., D_{10}, AUC) were calculated by one-way ANOVA.

14. REFERENCES

1. Adam J. F., Joubert A., Biston M. C., Charvet A. M., Peoc'h M., Le Bas J. F., Balosso J., Esteve F., Elleaume H. Prolonged survival of Fischer rats bearing F98 glioma after iodine-enhanced synchrotron stereotactic radiotherapy. Int. J. Radiat. Oncol. Biol. Phys. 64 (2006) 603–611.
2. Adams F. H., Norman A., Mello R. S., Bass D. Effect of radiation and contrast media on chromosomes. Preliminary report. Radiology 124 (1977) 823–826.
3. Afshar G., Jelluma N., Yang X., Basila D., Arvold N.D., Karlsson A., Yount G.L., Dansen T.B., Koller E., Haas-Kogan D.A. Radiation-induced caspase-8 mediates p53-independent apoptosis in glioma cells. Cancer Res. 66 (2006) 4223-32.
4. Allabashi R., Stach W., de la Escosura-Muniz A., Liste-Calleja L. and Merkoçi A. ICP-MS: a powerful technique for quantitative determination of gold nanoparticles without previous dissolving. J Nanopart Res 11 (2009) 2003-2011.
5. Aydogan B., Li J., Rajh T., Chaudhary A., Chmura S.J., Pelizzari C., Wietholt C., Kurtoglu M., Redmond P. AuNP-DG: deoxyglucose-labeled gold nanoparticles as X-ray computed tomography contrast agents for cancer imaging. Mol Imaging Biol 12 (2010) 463-467.
6. Biaglow J.E., Varnes M.E., Clark E.P., Epp E.R. The role of thiols in cellular response to radiation and drugs. Radiat Res. 95 (1983) 437-55.
7. Bohren C.F., Huffman D.R. Absorption and scattering of light by small particles. Wiley, NewYork (1983).

8. Boudaiffa B., Cloutier P., Hunting D., Huels M.A., Sanche L. Resonant formation of DNA strand breaks by low-energy (3 to 20 ev) electrons. Science 287 (2000) 1658-1660.
9. Boudou C., Balosso J., Esteve F., Elleaume H. Monte Carlo dosimetry for synchrotron stereotactic radiotherapy of brain tumors. Phys. Med. Biol. 50 (2005) 4841–4851.
10. Brenner D.J., Hlatky L.R., Hahnfeldt P.J., Huang Y., Sachs R.K. The linear-quadratic model and most other common radiobiological models result in similar predictions of time-dose relationships. Radiat Res. 150 (1998) 83-91.
11. Brun E., Cloutier P., Sicard-Roselli C., Fromm M., Sanche L. Damage induced to DNA by low-energy (0−30 ev) electrons under vacuum and atmospheric conditions. J Phy Chem B 113 (2009): 10008-10011.
12. Butterworth K.T., Coulter J.A., Jain S., Forker J., McMahon S.J., Schettino G., Prise K.M., Currell F.J., Hirst D.G. Evaluation of cytotoxicity and radiation enhancement using 1.9 nm gold particles: Potential application for cancer therapy. Nanotechnology 21 (2010) 295101.
13. Cai W., Gao T., Hong H., Sun J. Applications of gold nanoparticles in cancer nanotechnology. Nanotechnol Sci Appl 1 (2008) 17–32.
14. Callisen H.H., Norman A., Adams F.H. Absorbed dose in the presence of contrast agents during pediatric cardiac catheterization. Med. Phys. 6 (1979) 504–509 .
15. Carter J.D., Cheng N.N., Qu Y., Suarez G.D., Guo T. Nanoscale energy deposition by x-ray absorbing nanostructures. J. Phy. Chem. B 111 (2007) 11622-11625.

16. Chang M.Y., Shiau A.L., Chen Y.H., Chang C.J., Chen H.H., Wu C.L. Increased apoptotic potential and dose-enhancing effect of gold nanoparticles in combination with single-dose clinical electron beams on tumor-bearing mice. Cancer Sci 99 (2008) 1479-1484.
17. Chatterjee A. and Magee J.L. Theoretical investigation of the production of strand breaks in DNA by water radicals Radiat. Prot. Dosim. 13 (1985) 137-140.
18. Chen W. and Zhang J. Using nanoparticles to enable simultaneous radiation and photodynamic therapies for cancer treatment. J. Nanosci. Nanotechnol. 6 (2006) 1159-1166.
19. Chithrani B.D., Ghazani A.A. and Chan W.C. Determining the size and shape dependence of gold nanoparticle uptake into mammalian cells. Nano Lett 6 (2006) 662-668.
20. Chithrani D.B., Dunne M., Stewart J., Allen C., Jaffray D.A. Cellular uptake and transport of gold nanoparticles incorporated in a liposomal carrier. Nanomedicine 6 (2010) 161-169.
21. Chithrani D.B., Jelveh S., Jalali F., van Prooijen M., Allen C., Bristow R.G., Hill R.P., Jaffray D.A. Gold nanoparticles as a radiation sensitizer in cancer therapy. Radiat Res 173 (2010) 719-728.
22. Cho S.H. Estimation of tumor dose enhancement due to gold nanoparticles during typical radiation treatments: a preliminary Monte Carlo study. Phys. Med. Biol. 50 (2005) N163–N173.
23. Choi K.Y., Saravanakumar G., Park J.H., Park K. Hyaluronic acid-based nanocarriers for intracellular targeting: interfacial interactions with proteins in cancer. Colloids Surf B Biointerfaces. 99 (2012) 82-94.

24. Corde S., Joubert A., Adam J.F., Charvet A.M., Le Bas J.F., Estève F., Elleaume H., Balosso J. Synchrotron radiation-based experimental determination of the optimal energy for cell radiotoxicity enhancement following photoelectric effect on stable iodinated compounds. Br. J. Cancer 91(2004) 544–551.
25. Crow J.P. Dichlorodihydrofluorescein and dihydrorhodamine 123 are sensitive indicators of peroxynitrite in vitro: implications for intracellular measurement of reactive nitrogen and oxygen species. Nitric Oxide 1 (1997) 145-157.
26. Cuenca A.G., Jiang H., Hochwald S.N., Delano M., Cance W.G., Grobmyer S.R. Emerging implications of nanotechnology on cancer diagnostics and therapeutics. Cancer, 107 (2006) 459-466.
27. Das I.J. and Chopra K.L. Backscatter dose perturbation in kilovoltage photon beams at high atomic number interfaces. Med. Phys. 22 (1995) 767–773.
28. Das I.J. and Kahn F.M. Backscatter dose perturbation at high atomic number interfaces in megavoltage photon beams. Med. Phys. 16 (1989) 367–375.
29. Douglas B.G. and Fowler J.F. The effect of multiple small doses of X-rays on skin reactions in the mouse and a basic interpretation. Radiat Res 66 (1976) 401-26.
30. Dvorak H. F., Nagy J.A., Dvorak J.T., Dvorak A. M. Identification and characterization of the blood vessels of solid tumors that are leaky to circulating macromolecules. Am J. Pathol. 133 (1988) 95–109.
31. Fairchild R.G., Brill A.B., Ettinger K.V. Radiation enhancement with iodinated deoxyuridine. Invest. Radiol. 17 (1982) 407–416.
32. Franken N.A.P., Rodermond H.M., Stap J., Haveman J. and van Bree C. Clonogenic assay of cells in vitro. Nature Protocols 1 (2006) 2315.

33. Furnari F.B., Fenton T., Bachoo R.M., Mukasa A., Stommel J.M., Stegh A., Hahn W.C., Ligon K.L., Louis D.N., Brennan C., Chin L., DePinho R.A., Cavenee W.K. Malignant astrocytic glioma: genetics, biology, and paths to treatment. Genes Dev 21 (2007): 2683-2710.
34. Furuyama A., Kanno S., Kobayashi T., Hirano S. Extrapulmonary translocation of intratracheally instilled fine and ultrafine particles via direct and alveolar macrophage-associated routes. Arch Toxicol 83 (2009) 429-437.
35. Guillamo JS, Lisovoski F, Christov C, Le Guérinel C, Defer GL, Peschanski M, Lefrançois T. Migration pathways of human glioblastoma cells xenografted into the immunosuppressed rat brain. J Neurooncol. 52 (2001) 205-15.
36. Hainfeld J.F., Dilmanian F.A., Slatkin D.N. and Smilowitz H.M. Radiotherapy enhancement with gold nanoparticles. J Pharm Pharmacol 60 (2008) 977-985.
37. Hainfeld J.F., Dilmanian F.A., Zhong Z., Slatkin D.N., Kalef-Ezra J.A., Smilowitz H.M. Gold nanoparticles enhance the radiation therapy of a murine squamous cell carcinoma. Phys Med Biol 55 (2010) 3045-3059.
38. Hainfeld J.F., Slatkin D.N. and Smilowitz H.M. The use of gold nanoparticles to enhance radiotherapy in mice. Phys Med Biol 49 (2004) 309-315.
39. Hainfeld J.F., Slatkin DN., Focella T.M., Smilowitz H.M. Gold nanoparticles: a new X-ray contrast agent. British Journal of Radiology 79 (2006) 248–253.
40. Han Wei and Yu K. N. onizing Radiation, DNA Double Strand Break and Mutation. Advances in Genetics Research. Vol. 4, Nova (2010).
41. Henderson L.M. and Chappell J.B. Dihydrorhodamine 123: a fluorescent probe for superoxide generation? Eur J Biochem 217 (1993) 973-980.

42. Herold D.M., Das I.J., Stobbe C.C., Iyer R.V., Chapman J.D. Gold microspheres: a selective technique for producing biologically effective dose enhancement. Int. J. Radiat. Biol. 76 (2000) 1357–1364.
43. Hoelzinger D.B., Demuth T., Berens M.E. Autocrine factors that sustain glioma invasion and paracrine biology in the brain microenvironment. J Natl Cancer Inst. 99 (2007) 1583-93.
44. Jain S., Coulter J.A., Hounsell A.R., Butterworth K.T., McMahon S.J., Hyland W.B., Muir M.F., Dickson G.R., Prise K.M., Currell F.J., O'Sullivan J.M., Hirst D.G. Cell-specific radiosensitization by gold nanoparticles at megavoltage radiation energies. Int J Radiat Oncol Biol Phys 79 (2011) 531-539.
45. Jelveh S. and Chithrani D.B. Gold Nanostructures as a platform for combinational therapy in future cancer therapeutics. Cancers 3 (2011) 1081-1110.
46. Jiao P.F., Zhou H.Y., Chen L.X., Yan B. Cancer-targeting multifunctionalized gold nanoparticles in imaging and therapy. Curr Med Chem 18 (2011) 2086-2102.
47. Judy J.D., Unrine J.M. and Bertsch P.M., Evidence for biomagnification of gold nanoparticles within a terrestrial food chain. Environ Sci Technol 45 (2011) 776-781.
48. Julien O., Beadle J.R., Magee W.C., Chatterjee S., Hostetler K.Y., Evans D.H., Sykes B.D. Solution structure of a DNA duplex containing the potent anti-poxvirus agent cidofovir. J Am Chem Soc. 133 (2011) 2264-74.
49. Karnas S.J., Yu E., McGarry R.C., Battista J.J. Optimal photon energies for IUdR K-edge radiosensitization with filtered X-ray and radioisotope sources. Phys. Med. Biol. 44 (1999) 2537–2549.

50. Kim J.K., Seo S.J., Kim K.H., Kim T.J., Chung M.H., Kim K.R., Yang T.K. Therapeutic application of metallic nanoparticles combined with particle-induced x-ray emission effect. Nanotechnology 21 (2010) 425102.
51. Kong T., Zeng J., Wang X., Yang X., Yang J., McQuarrie S., McEwan A., Roa W., Chen J., Xing J.Z. Enhancement of radiation cytotoxicity in breast-cancer cells by localized attachment of gold nanoparticles. Small 4 (2008) 1537-1543.
52. Kreibig U., Vollmer M. Optical Properties of Metal Clusters. Springer-Verlag, Berlin (1995).
53. Kumar A., Ma H., Zhang X., Huang K., Jin S., Liu J., Wei T., Cao W., Zou G., Liang X.J. Gold nanoparticles functionalized with therapeutic and targeted peptides for cancer treatment. Biomaterials 33 (2012) 1180-1189.
54. Lefranc F, Brotchi J, Kiss R. Possible future issues in the treatment of glioblastomas: special emphasis on cell migration and the resistance of migrating glioblastoma cells to apoptosis. J Clin Oncol 23 (2005) 2411-2422.
55. Leung M.K., Chow J.C., Chithrani B.D., Lee M.J., Oms B., Jaffray D.A. Irradiation of gold nanoparticles by x-rays: Monte Carlo simulation of dose enhancements and the spatial properties of the secondary electrons production. Med Phys 38 (2011) 624-631.
56. Liu C.J., Wang C.H., Chen S.T., Chen H.H., Leng W.H., Chien C.C., Wang C.L., Kempson I.M., Hwu Y., Lai T.C., Hsiao M., Yang C.S., Chen Y.J. Margaritondo G. Enhancement of cell radiation sensitivity by pegylated gold nanoparticles. Phys Med Biol 55 (2010) 931-945.
57. Maeda H., Wu J., Sawa T., Matsumura Y., Hori K. Tumor vascular permeability and the EPR effect in macromolecular therapeutics: a review. J. Control. Release 65 (2000) 271–284.

58. Martin de Llano J.J., Andreu E.J. and Knecht E. Use of inductively coupled plasma-mass spectrometry for the quantitation of the binding and uptake of colloidal gold-low-density lipoprotein conjugates by cultured cells. Anal Biochem 243 (1996) 210-217.
59. Matsuda M., Yamamoto T., Ishikawa E., Nakai K., Zaboronok A., Takano S., Matsumura A. Prognostic factors in glioblastoma multiforme patients receiving high-dose particle radiotherapy or conventional radiotherapy. Br J Radiol, 84 (2011) S54-60.
60. Matsudaira H., Ueno A.M., Furuno I. Iodine contrast medium sensitizes cultured mammalian cells to X-rays but not to gamma rays. Radiat. Res. 84 (1980) 144–148.
61. Merritt A.J., Allen T.D., Potten C.S., Hickman J.A. Apoptosis in small intestinal epithelial from p53-null mice: evidence for a delayed, p53-independent G2/M-associated cell death after gamma-irradiation. Oncogene. 14 (1997) 2759-66.
62. Montenegro M., Nahar S.N., Pradhan A.K., Huang K., Yu Y. Monte Carlo simulations and atomic calculations for auger processes in biomedical nanotheranostics. J Phys Chem A 113 (2009) 12364-12369.
63. Murayama C., Suzuki A., Sato C., Tanabe Y., Shoji T., Miyata Y., Nishio A., Suzuki T., Sakaguchi M., Mori T. Radiosensitization by a new potent nucleoside analog: 1-(1′,3′,4′-trihydroxy-2′-butoxy)methyl-2-nitroimidazole(RP-343). Int. J. Radiat. Oncol. Biol. Phys. 26 (1993) 433–443.
64. Nath R., Bongiorni P., Rockwell S. Iododeoxyuridine radiosensitization by low- and high-energy photons for brachytherapy dose rates Radiat. Res. 124 (1990) 249–258.

65. Nishioka A., Ohizumi Y., Lam G.K., Pickles T.A., Chaplin D.J., Ogawa Y., Inomata T., Yoshida S. The effects of nicotinamide plus carbogen or pions for microscopic SCCVII tumors. Oncol. Rep. 6 (1999) 583–586.
66. Pan Y., Neuss S., Leifert A., Fischler M., Wen F., Simon U., Schmid G., Brandau W., Jahnen-Dechent W. Size-dependent cytotoxicity of gold nanoparticles. Small 3 (2007) 1941-1949.
67. Poludniowski G.G. and Evans P.M. Calculation of x-ray spectra emerging from an x-ray tube. Part I. electron penetration characteristics in x-ray targets. Med Phys 34 (2007) 2164-2174.
68. Poludniowski G.G., Landry G., DeBlois F., Evans P.M., Verhaegen F. SpekCalc: a program to calculate photon spectra from tungsten anode x-ray tubes. Phys Med Biol 54 (2009) 433-438.
69. Popovtzer R., Agrawal A., Kotov N.A., Popovtzer A., Balter J., Carey T.E., Kopelman R. Targeted gold nanoparticles enable molecular CT imaging of cancer. Nano Lett 8 (2008) 4593-4596.
70. Pradhan A.K., Nahar S.N., Montenegro M., Yu Y., Zhang H.L., Sur C., Mrozik M., Pitzer R.M. Resonant X-ray enhancement of the Auger effect in high-Z atoms, molecules, and nanoparticles: potential biomedical applications. J Phys Chem A 113 (2009) 12356-12363.
71. Rahman W.N., Bishara N., Ackerly T. He C.F., Jackson P., Wong C., Davidson R., Geso M. Enhancement of radiation effects by gold nanoparticles for superficial radiation therapy. Nanomedicine 5 (2009) 136-142.
72. Rao J. Shedding light on tumors using nanoparticles. ACS Nano 2 (2008) 1984-1986.

73. Regulla D.F., Hieber L.B., Seidenbusch M. Physical and biological interface dose effects in tissue due to X-ray-induced release of secondary radiation from metallic gold surfaces Radiat. Res. 150 (1998) 92–100.
74. Regulla D.F., Schmid E., Friedland W., Panzer W., Heinzmann U., Harder D. Enhanced values of the RBE and H ratio for cytogenetic effects induced by secondary electrons from an X-irradiated gold surface. Radiat. Res. 158 (2002) 505–515.
75. Reuveni T., Motiei M., Romman Z., Popovtzer A., Popovtzer R. Targeted gold nanoparticles enable molecular CT imaging of cancer: an in vivo study. Int J Nanomedicine 6 (2011) 2859-64.
76. Robar J.L., Riccio S.A., Martin M.A. Tumor dose enhancement using modified megavoltage photon beams and contrast media. Phys. Med. Biol. 47 (2002) 2433–2449.
77. Rodriguez-Fernandez J., Perez-Juste J., Mulvaney P., Liz-Marzan L. M. Spatially-directed oxidation of gold nanoparticles by Au(III)-CTAB complexes. J. Phys. Chem. B. 109 (2005) 14 257–14 261.
78. Roeske J.C., Nunez L., Hoggarth M., Labay E., Weichselbaum R.R. Characterization of the theoretical radiation dose enhancement from nanoparticles. Technol. Cancer Res. Treat. 6 (2007) 395–402.
79. Rose J.H., Norman A., Ingram M., Aoki C., Solberg T., Mesa A. First radiotherapy of human metastatic brain tumors delivered by a computerized tomography scanner (CTRx). Int. J. Radiat. Oncol. Biol. Phys. 45 (1999) 1127–1132.
80. Sanche L. Beyond radical thinking. Nature 461 (2009) 358-359.

81. Sanche L. Nanoscopic aspects of radiobiological damage: Fragmentation induced by secondary low-energy electrons. Mass Spectrom Rev. 21(2002):349-69.
82. Santos Mello R., Callisen H., Winter J., Kagan A.R., Norman A. Radiation dose enhancement in tumors with iodine. Med. Phys. 10 (1983) 75–78.
83. Scheffer A., Engelhard C., Sperling M., Buscher W. ICP-MS as a new tool for the determination of gold nanoparticles in bioanalytical applications. Anal Bioanal Chem 390 (2008) 249-252.
84. Setsukinai K., Urano Y., Kakinuma K., Majima H.J., Nagano T. Development of novel fluorescence probes that can reliably detect reactive oxygen species and distinguish specific species. J Biol Chem 278 (2003) 3170-3175.
85. Shibamoto Y., Zhou L., Hatta H., Mori M., Nishimoto S. I. In vivo evaluation of a novel antitumor prodrug, 1-(2′-oxopropyl)-5-fluorouracil (OFU001), which releases 5-fluorouracil upon hypoxic irradiation. Int J Radiat Oncol Biol Phys 49 (2001) 407–413.
86. Shibamoto Y., Zhou L., Hatta H., Mori M., Nishimoto S. I. In vivo evaluation of a novel antitumor prodrug, 1-(2′-oxopropyl)-5-fluorouracil (OFU001), which releases 5-fluorouracil upon hypoxic irradiation. Int J Radiat Oncol Biol Phys 49 (2001) 407–413.
87. Soh N. Recent advances in fluorescent probes for the detection of reactive oxygen species. Anal Bioanal Chem 386 (2006) 532-543.
88. Spiers F.W. The influence of energy absorption and electron range on dosage in irradiated bone. Br. J. Radiol. 22 (1949) 521–533.
89. Trono J.D., Mizuno K., Yusa N., Matsukawa T., Yokoyama K., Uesaka M. Size, concentration and incubation time dependence of gold nanoparticle uptake into

pancreas cancer cells and its future application to X-Ray Drug Delivery System. J Radiat Res 52 (2011) 103-109.

90. Wang C.-R., Nguyen J., Lu Q.-B. Bond breaks of nucleotides by dissociative electron transfer of nonequilibrium prehydrated electrons: A new molecular mechanism for reductive DNA damage. J. Am. Chem. Soc. 131 (2009) 11320-11322.
91. Wei Z. and Zamborini F.P. Directly monitoring the growth of gold nanoparticle seeds into gold nanorods. Langmuir 20 (2004) 11 301–11 304.

参　考　論　文

http://dx.doi.org/10.1166/nnl.2013.1646

LIST OF PUBLICATIONS

1. Proton beam irradiation stimulates migration and invasion of human U87 malignant glioma cells. Zaboronok A, Isobe T, Yamamoto T, Sato E, Takada K, Sakae T, Tsurushima H, Matsumura A. J Radiat Res 2013 Nov 1. [Epub ahead of print].
2. Size-dependent radiosensitization effects of gold nanoparticles on human U251 malignant glioma cells. Zaboronok A, Tsurushima H, Yamamoto T, Isobe T, Takada K, Sakae T, Yoshida F, Matsumura A. Nanosci Nanotechnol Lett 5:990-994, 2013.
3. Spinal dural arteriovenous fistula with lipomyelodysplasia. Sato M, Takigawa T, Shiigai M, Tamura G, Masumoto T, Nakai Y, Zaboronok A, Tsurushima H, Matsumura A. Neurol Med Chir (Tokyo). 53(2):107-109, 2013.
4. Acute subdural hematoma without subarachnoid hemorrhage caused by ruptured A1-A2 junction aneurysm. Case report. Takada T, Yamamoto T, Ishikawa E, Zaboronok A, Kujiraoka Y, Akutsu H, Ihara S, Nakai K, Matsumura A. Neurol Med Chir (Tokyo). 52(6):430-434, 2012.
5. Elevated diffusion anisotropy in gray matter and the degree of brain compression. Osuka S, Matsushita A, Ishikawa E, Saotome K, Yamamoto T, Marushima A, Satou N, Zaboronok A, Masumoto T, Matsumura A. J Neurosurg. 117(2):363-371, 2012.
6. Dual-port technique in navigation-guided endoscopic resection for intraparenchymal brain tumor. Masuda Y, Ishikawa E, Takahashi T, Ihara S, Yamamoto T, Zaboronok A, Matsumura A. Surg Neurol Int. 3:35, 2012.
7. Glioma immunotherapy with combined autologous tumor cell and endothelial cell vaccine in vivo. Sakamoto N, Uemae Y, Ishikawa E, Takano S, Nakai K, Yamamoto T, Zaboronok A, Matsumura A. Neurol Med Chir (Tokyo). 52(4):194-201, 2012.
8. Navigation-guided endoscopic biopsy for pathological diagnosis for

intraparenchymal pure germinoma near the ventricular trigone. Onuma K, Ishikawa E, Matsuda M, Shibata Y, Satomi K, Yamamoto T, Zaboronok A, Takano S, Matsumura A. Surg Neurol Int. 3:9, 2012.

9. Navigation-guided endoscopic biopsy for intraparenchymal brain tumor. Tsuda K, Ishikawa E, Zaboronok A, Nakai K, Yamamoto T, Sakamoto N, Uemae Y, Tsurubuchi T, Akutsu H, Ihara S, Ayuzawa S, Takano S, Matsumura A. Neurol Med Chir (Tokyo). 51(10):694-700, 2011.

10. Prognostic factors in glioblastoma multiforme patients receiving high-dose particle radiotherapy or conventional radiotherapy. Matsuda M, Yamamoto T, Ishikawa E, Nakai K, Zaboronok A, Takano S, Matsumura A. Br J Radiol. 84 Spec No 1:S54-60, 2011.

11. The status of Tsukuba BNCT trial: BPA-based boron neutron capture therapy combined with X-ray irradiation. Yamamoto T, Nakai K, Nariai T, Kumada H, Okumura T, Mizumoto M, Tsuboi K, Zaboronok A, Ishikawa E, Aiyama H, Endo K, Takada T, Yoshida F, Shibata Y, Matsumura A. Appl Radiat Isot. 69(12):1817-1818, 2011.

12. Proton magnetic resonance spectroscopy findings of hemangioblastoma. Isobe T, Yamamoto T, Akutsu H, Anno I, Shiigai M, Zaboronok A, Masumoto T, Takano S, Matsumura A. Jpn J Radiol. 28(4):318-321, 2010.

13. Intracellular uptake of a new boronated porphyrin EC032. Tsurubuchi T, Yamamoto T, Nakai K, Zaboronok A, Yoshida F, Miyakawa M, Shirakawa M, Yamamoto Y, Matsuda M, Matsumura A. Appl Radiat Isot. 67(7-8 Suppl):S94-96, 2009.

14. Feasibility of boron neutron capture therapy for malignant spinal tumors. Nakai K, Kumada H, Yamamoto T, Tsurubuchi T, Zaboronok A, Matsumura A. Appl Radiat Isot. 67(7-8 Suppl):S43-46, 2009.

15. Boron neutron capture therapy for newly diagnosed glioblastoma: a pilot study in Tsukuba. Yamamoto T, Nakai K, Tsurubuchi T, Matsuda M, Shirakawa M, Zaboronok A, Endo K, Matsumura A. Appl Radiat Isot. 67(7-8 Suppl):S25-26, 2009.

16. The optimization of fluorescence imaging of brain tumor tissue differentiated from brain edema-in vivo kinetic study of 5-aminolevulinic acid and talaporfin sodium. Tsurubuchi T, Zaboronok A, Yamamoto T, Nakai K, Yoshida F, Shirakawa M, Matsuda M, Matsumura A. Photodiagnosis Photodyn Ther. 6(1):19-27, 2009.